Applied Energy 379 (2025) 124950

Contents lists available at ScienceDirect

Applied Energy

journal homepage: www.elsevier.com/locate/apenergy

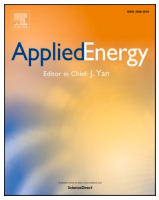

Assessment of electricity production and coastal protection of a nearshore 500 MW wave farm in the north-western Portuguese coast

D. Clemente [a,b,*], V. Ramos [a,b], F. Teixeira-Duarte [a,b], F.V.C. Taveira-Pinto [a,b], P. Rosa-Santos [a,b], F. Taveira-Pinto [a,b]

[a] Department of Civil Engineering, Faculty of Engineering of the University of Porto, Rua Dr. Roberto Frias, S/N, 4200-465 Porto, Portugal
[b] Interdisciplinary Centre of Marine and Environmental Research (CIIMAR), Leixões Cruise Terminal, Av. General Norton de Matos S/N, 4450-208, Matosinhos, Portugal

HIGHLIGHTS

- Numerical study with SNL-SWAN on a dual wave farm for Esposende, Portugal;
- Power absorption and local impact analysis of farm setup, rating and marine climate;
- Two parks with 75 units each deployed to avoid local marine space restrictions;
- Representative local wave climate summarized through a K-Means clustering technique;
- Overall, the "W" 280° 1.5D setup, rated at 3.332 MW, exhibited the best results;

ARTICLE INFO

Keywords:
Ocean renewable energy
Oscillating wave surge converter farm
Portuguese shoreline
Coastal protection
Marine space usage
SNL-SWAN numerical model

ABSTRACT

Wave energy can contribute towards the "green" energy transition, but complementary applications like coastal protection are equally pertinent. However, viable commercialization should entice large wave energy farms of significant capacity, which may raise conflicts with coastal industries and/or protected areas. Such matters are addressed in this paper's numerical case study of a dual wave farm for a nearshore Portuguese site. It incorporates two parks of 75 bottom-fixed oscillating flap units, each. The farm's configuration, orientation, layout, and rating were evaluated for varying wave conditions and water levels, based on a statistically representative clustering technique. The farm's location was selected to minimize marine space conflicts. The numerical modelling was executed with SNL-SWAN, from which it was found that a staggered configuration – "W" – would yield better results than an aligned configuration – "III". The "shadowing" effect of one park onto the other was equally observed, but with limited impact. Greater farm unit spacing and rated power benefited the annual energy production, with values of nearly 345 GWh/yr being achieved. However, the capacity factors were generally greater for lower power ratings, as pondered mean values varied between 0.078 (3.332 MW) to 0.144 (1 MW). Wave power absorption ratios between wave farms and cumulative standalone units (*q-factors*) were always below 1, pointing towards a destructive interference pattern. Important significant wave height reductions were observed (above 30 %, at times), albeit increments were punctually identified near two shallow water areas. Lastly, increasing the tidal level did not impact the farm's performance considerably, but benefited the nearshore impact.

1. Introduction

Several wave energy converter (WEC) concepts are reaching high Technological Readiness Levels (TRLs), aimed at sea trial demonstrations. According to Ocean Energy Systems (OES) [1,2], nearly 25 MW were installed between 2010 and 2022, 165 kW of which in 2022 alone. About half of this cumulative capacity originates from Europe, with 400 kW currently at sea. Such efforts originate from the highly

* Corresponding author at: Department of Civil Engineering, Faculty of Engineering of the University of Porto, Rua Dr. Roberto Frias, S/N, 4200-465 Porto, Portugal.
E-mail address: up603010@up.pt (D. Clemente).

https://doi.org/10.1016/j.apenergy.2024.124950
Received 1 July 2024; Received in revised form 23 October 2024; Accepted 15 November 2024
Available online 23 November 2024

dense, predictable, and abundant nature of wave energy. Under anthropogenic climate change, additional R&D ought to bolster the "green" energy transition by expanding the installed capacity and wave energy output.

Portugal's coastline is directly exposed to the high-energy wave climate of the Atlantic Ocean, which entices engineering challenges from constructing protective structures (e.g., breakwaters at seaports) to studying hydrodynamic interactions with shorelines (e.g., erosion and flooding) [3]. Even so, with a mean annual wave power of 15 to 35 kW/m, there is interest in giving wave energy a useful purpose [4]. Also, in 2023, over 60 % of Portugal's electricity (continent) originated from renewable energy sources (RES) – mainly hydropower, wind and solar [5]. By incorporating wave energy, Portugal could become virtually self-sufficient or even an electricity exporter, pivotal milestones to the national and European strategies for "green" energy transition and autonomy [6]. This energy could also power marine niche markets such as offshore aquaculture and desalination [7], both of high national potential [8,9].

Studies on the Portuguese nearshore and the entire NW Iberian Peninsula reveal a substantial wave energy resource. Iglesias et al. [10] conducted a 10-year hindcast simulation along the offshore coast of Galicia, finding annual wave energy values between 128 and 439 MWh/m, with average wave power from 15 to 50 kW/m. Pontes et al. [11] developed an online atlas of the nearshore Portuguese wave energy resource, using advanced models to find typical values of 25 kW/m at exposed sites. Rusu and Guedes Soares [12] simulated wave power density for various case studies, highlighting higher energy resource near capes and Viana do Castelo. Mota and Pinto [13] performed a 15-year hindcast using WAVEWATCH III, which indicated an average offshore wave power from 28.11 to 30.90 kW/m. Nearshore wave power ranged from 24.56 to 25.91 kW/m, with the highest annual potential near Viana do Castelo and Leixões at 223 MWh/m. Current projections also suggest that wave energy will remain significant in the next decades. However, future wave energy extraction will depend on parameters beyond wave power intensity, such as temporal and monthly variability, which are related with wave energy stability. Rusu's analysis for 2026–2045 under the RCP4.5 scenario showed no significant differences in wave power compared to 2001–2020 during Spring and Autumn, but still identified a decrease in Summer and an increase in Winter [14]. Majidi et al. [3] studied the impact of climate change on wave energy under the RCP8.5 scenario, finding a decreasing trend, from 15.1 to 7.2 kW/m, on the maximum annual power ranges due to changes in atmospheric circulation and ocean temperature gradients, impacting WEC design. Arguilé-Pérez et al. [15] assessed WEC suitability in northwestern Spain, concluding that the Atargis WEC is adequate for intermediate-deep waters and the WaveRoller® for shallow nearshore areas. Thus, it becomes clear that the West Iberian coastal areas, including those along the Portuguese nearshore, possess a substantial wave energy resource that can be exploited by existing WEC technologies, though long-term changes should be considered.

Recently, several companies deployed (or foresee deploying) WEC devices in Portuguese waters: AW-Energy's WaveRoller® (350 kW), CorPower's C4 (1.2 MW, 300 kW/unit) and Eco Wave Power's energy station (20 MW) [16–18]. Furthermore, the Portuguese Government is promoting an auction for offshore RES – 2 GW by 2030 [19] –, to which adds a sizeable nearshore resource. Though mainly focused on offshore wind, there is room for co-location with wave energy [20,21] or even WEC hybridization approaches. On the former, there are synergies that range from dual energy conversion and, overall, lower costs (especially for wave energy), to operational safety and accessibility enhancement for offshore wind turbines, with the WEC park acting as wave attenuator through energy absorption (leeward wake effect upon the offshore wind farm) [22,23]. On the latter, one can find in literature numerous hybridized case studies, including pitching/rolling WEC incorporation with triboelectric nanogenerators – Salter's Duck [24] and *E*-Motions [25] –, pendulum-gyroscopic systems with multi-mode operation for omnidirectional waves – SWINGO [26] –, or even hybridized WECs for integration into breakwaters – Oscillating Water Column and Overtopping [27] –, among others [28,29]. Extending from the wave-wind co-location benefits, WEC farms can serve a secondary purpose of coastal protection through wave attenuation and, consequently, sheltering of sensitive shorelines [30,31]. However, literature studies on this prospect often follow a simplified approach to wave farm modelling (e.g., invariant transmission coefficient, fixed power ratings/matrices and/or limited farm configurations), assume a small number of WEC units and/or neglect local marine space restrictions.

With limited field data, standard techniques for developing WECs revolve around physical and numerical modelling. The latter is quite suitable for assessing multi-variable combinations through wave propagation models (WPMs). These robust, high-fidelity tools can be adapted to forecast wave climates, WEC farm energy outputs and local impact (near-field and far-field effects) [32,33]. Some recent applications even resort to data-driven algorithms, from sea-state prediction to WEC park layout optimization [34,35]. Even so, several studies still resort to physics-driven codes such as Simulating WAves Nearshore (SWAN) [36], including the Delft3D [37] and SNL-SWAN [38] upgrades:

- Evaluating the impact of a Wave Dragon park with varying layouts in Óbidos, Portugal. The study resorted to SWAN and data from the European Space Agency and ERA5, exhibiting noteworthy significant wave height H_s attenuation and current pattern shifts [39];
- Application of SNL-SWAN to an oscillating wave surge converter (OWSC) park for layout and energy production optimization, complemented by an assessment of its influence on local wave conditions. The case study region – Almagreira beach, Portugal – was the installation site of the OWSC WaveRoller®, in 2019, thus providing a realistic background [40,41];
- Assessment of multiple WEC concept farms, including OWSCs, with SNL-SWAN [42,43]. These studies include software parameter sensitivity, techno-economic analysis, shoreline evolution and influence on local hydrodynamics. In [44], the Oyster 2 OWSC could absorb up to 34.65 GWh/yr in the Sicilian Channel. With 100 units, reductions of up to 30 % were reported in [45] for the wave height and associated near-bottom orbital velocities (Monterey Bay and Santa Cruz, USA);
- A multi-criteria decision making tool, supported by SNL-SWAN, for co-located offshore wind and wave energy [23]. The selected WEC – CECO – is conceptually different from OWSCs, but the case study region was Viana do Castelo, Portugal. This work also features energy and local farm impact metrics, grid resolution convergence and statistical sea-state selection for a large farm.

Even so, there is a clear knowledge gap going from academic to more applied studies. Most literature works assume a limited number of WECs, resort to representative sea-state methodologies that disregard a sizeable portion of the data (e.g., "bin" methodology"), oversimplify wave-structure interactions and energy absorption (e.g., fixed transmission coefficient), and/or ignore marine space restrictions that, regardless of the quality of the research, would imply conflicts capable of jeopardizing the WEC farm's viability. To tackle these gaps, this paper seeks to *i*) propose an integrated, yet innovative methodology that combines marine space usage, statistical selection of representative sea-states, and multi-criteria evaluation of solutions for a high-TRL OWSC farm, assisted by the state-of-the-art WPM SNL-SWAN; *ii*) employ validated energy and wave parameter-based metrics to evaluate the farm's performance and local nearshore influence for distinct layouts, ratings and wave conditions; and *iii*) provide an in-depth approach and database for other researchers to replicate in their studies. The latter enables follow-up studies on coastal morphodynamical evolution and/or marine aquaculture for the case study region, in Northwest Portugal. While most studies focus solely on one or two of these topics, this paper congregates a multi-step, yet realistic proposal that simultaneously considers a large

number of WECs and installed capacity, a robust statistical procedure for the local wave conditions, and actual marine space restrictions.

The paper follows this structure: Section 2 details the case study region, selected OWSC technology, local wave climate, bathymetry and marine space restrictions, followed by the simulation plan and model configuration; Section 3 describes the theoretical background underlying the SNL-SWAN software, as well as considerations on model accuracy, validation and convergence; Section 4 highlights the main results, supported by metrics on energy output and nearshore effect; Section 5 discusses the proposed solutions and provides complementary remarks on the study's contributions and limitations; and Section 6 summarizes the study's key outcomes, whilst providing practical considerations and recommendations.

2. Materials and methods

In this section, the case study region is described in detail. The selected case study variables are also provided and discussed, from local wave conditions to tidal levels and marine space restrictions. The WEC technology and power matrix are equally addressed. The baseline proposal for the farm's layout is provided at the end of Section 2, based on the characteristics of the case study region and WEC type.

2.1. Case study overview

The case study region is the nearshore marine space at Esposende, Portugal, Fig. 1. Given its Northwestern location, the region exhibits a remarkable wave energy resource, even near the shoreline. In fact, it is bordered by Viana do Castelo (North) and Aguçadoura (South), which are prime locations for offshore marine renewable energy, including wave energy [4,23].

The region is characterized by natural and artificial coastal protection elements, such as the Ofir sandspit (2.1 km long), two longitudinal rubble-mound dikes and one groyne located in the river mouth. However, the interactions between waves, tides and river discharges play an important role on erosion and accretion processes near the river mouth. Thus, Ofir sandspit is highly sensitive when those dynamics occur with greater intensity. Over the past years, the fragile sandspit has lost a huge amount of sand, resulting in yearly shape changes, constant erosion at the sandspit's head and accretion in the navigation channel.

A recent rehabilitation study [46] provided a preliminary assessment on a new layout of coastal protection, based on low-crested detached breakwaters. Here, we propose a WEC farm as an alternative/complement to the solutions in [46] – "hard" (detached breakwater and dikes) and "living" (nature-based). A WEC farm can attenuate the high-energy wave climate whilst producing renewable electricity. The deployment site must be carefully selected, so that a balanced compromise exists between accommodating marine space restrictions, mitigating eventual impacts on local ecosystems, and maximizing the farm's dual performance.

2.2. Wave climate and tidal levels characterization

Fig. 2 shows the time series of valid hourly data points between January 1990 and December 2020, with negligible gaps over the 31-year period. The data was obtained from the Esposende sandspit rehabilitation study and a regional model (see Section 3.3), with the maritime conditions being in agreement with other sources [47,48].

The global average conditions revealed that the most frequent H_s are 1 to 2 m (over 44 % of occurrences), and that little over 2 % of the occurrences corresponds to storm conditions (above 5 m, maximum H_s of 9.2 m). Regarding the peak wave period T_p, about 88 % of the values are between 6 and 14 s, with an average of about 10.5 s. Finally, about 83 % of wave direction *Dir* occurrences relate to the NW-W octants (mean value of about 294°) [46,49]. The average seasonal conditions showed clear differences between the Summer (April to September) and Winter (October to March) periods, with the latter having the highest average monthly values of H_s.

Considering the tidal variation on the Northern Portuguese coast – semi-diurnal astronomical tides –, Table 1 shows real data available at [46,49]: highest tide *HT* (highest astronomical plus meteorological tides), high tide water springs *HTWS*, mean sea level *MSL* and low tide water springs *LTWS*. All levels are set with respect to the national hydrographic zero level *ZH*.

2.3. Local bathymetry and geomorphology restrictions

According to the Directorate-General for Natural Resources, Safety and Maritime Service's (DGRM) geoportal, the Esposende nearshore is characterized by several metasedimentary rock outcrops [50], such as Cavalos de Fão and Pena, which, alongside gravel and sediment deposits, induce wave diffraction and refraction. They reduce the wave energy acting on the sandspit and nearby beaches, whilst serving as habitats for various marine species (see Section 2.5.1), and ought to be

Fig. 1. – Location of Esposende, in Portugal, adapted from google earth (case study area approximately at 41°33′19″ N, 8°49′50″ W).

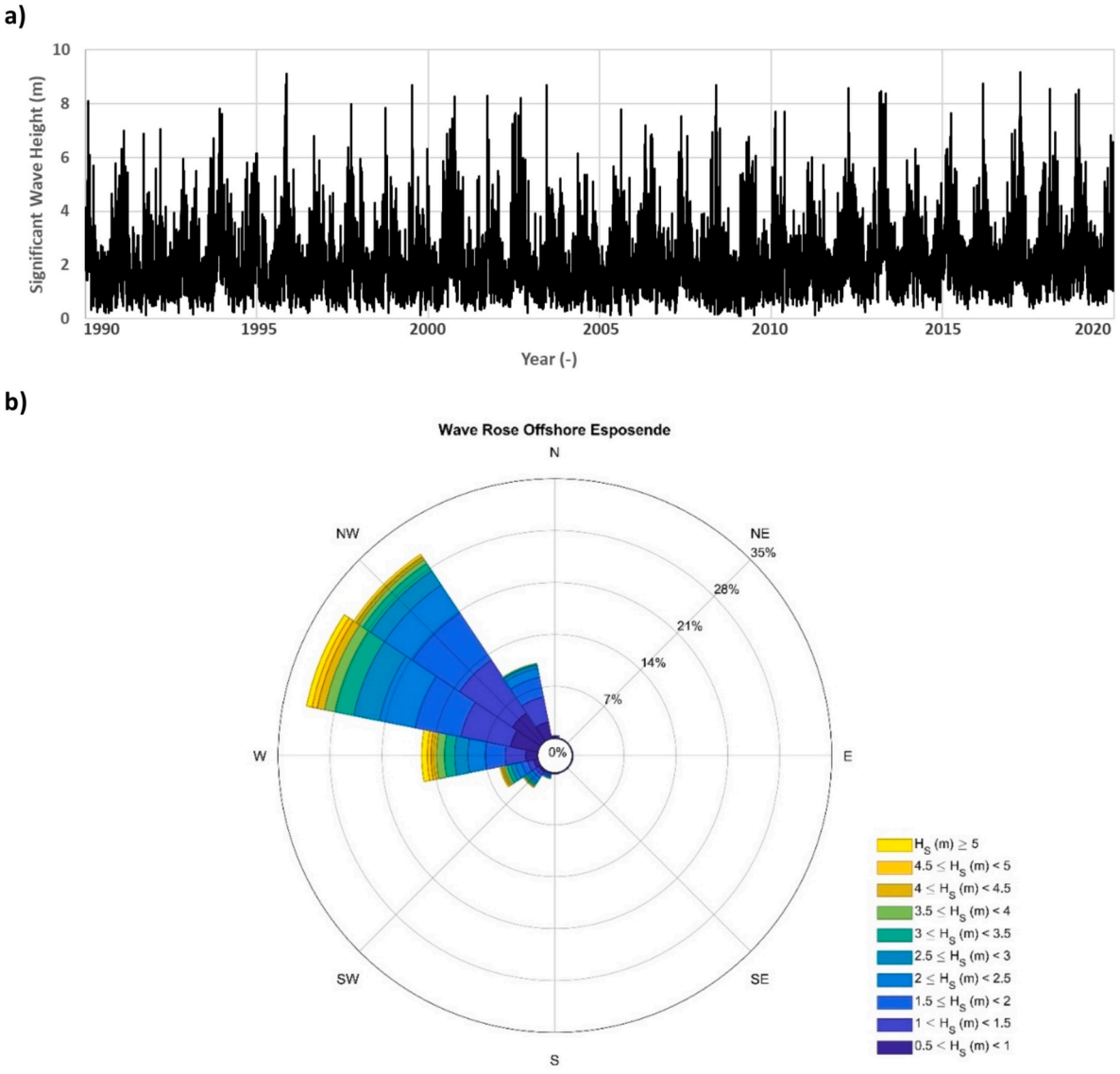

Fig. 2. – Maritime conditions from [46] (a), represented by a wave rose (b), adapted from [48]. (For interpretation of the references to colour in this figure legend, the reader is referred to the web version of this article.)

Table 1
– Approximate tidal levels from [46,49].

ZH (national)	*LTWS (min)*	*MSL*	*HTWS (max)*	*HT (extreme)*
+0.00 m	+0.50 m	+2.00 m	+3.50 m	+4.50 m

preserved [50,51]. They are equally pertinent upon establishing a suitable foundation for the WECs, as a rocky seabed mitigates issues regarding scouring and sediment accretion. Inadequate seabed areas or sites of interest, from a conservation perspective, can also be identified and avoided.

Regarding bathymetry, several marine lowlands and steep seabed profiles were identified, mainly in the 10–15 m depth transition (about 3 km from the shoreline). Based on data from the Hydrographic Institute (HI) and DGRM [50,52], water depths of up to 50 m are reported at nearly 3.5 nautical miles from the coast, Fig. 3. This conditions the viability of WEC technologies, given their specific operational depths. Furthermore, flat seabed surfaces may require fewer dredging works and provide more even/uniform foundations. This reduces installation costs and minimizes the impact on the natural seabed. In fact, there is a dredging area near Cavalos de Fão that ought to be avoided, as well.

In DGRM's geoportal [50], an area composed of sand and gravel has been identified at about 1 nautical mile off the coast. Furthermore, there are "strategic sediment management areas" going West and Southwest of the river mouth, to which add surface sediments identified in HI's chart for the Portuguese Continental Shelf – Fig. 3's "circalittoral fine sand" or "circalittoral muddy sand". There are also dredging regions that can not only restrict the available areas for WEC farm deployment, but also lead to sediment accretion issues.

As stated previously, there are important accretion and erosion occurrences at the access channel and along the Ofir sandspit, respectively. These reflect the unstable balance between river flows from Cávado, a longshore current from the North and prevailing wave action from the North to West quadrants. Hence, a WEC farm ought to mitigate these occurrences whilst avoiding the strategic sediment areas of interest.

2.4. Oscillating wave surge converter: device selection

Coastline proximity promotes accessibility, costs savings by reducing electric cable extensions, and can influence a WEC farm's wake effect [31], which is crucial towards the coastal protection purpose. While the

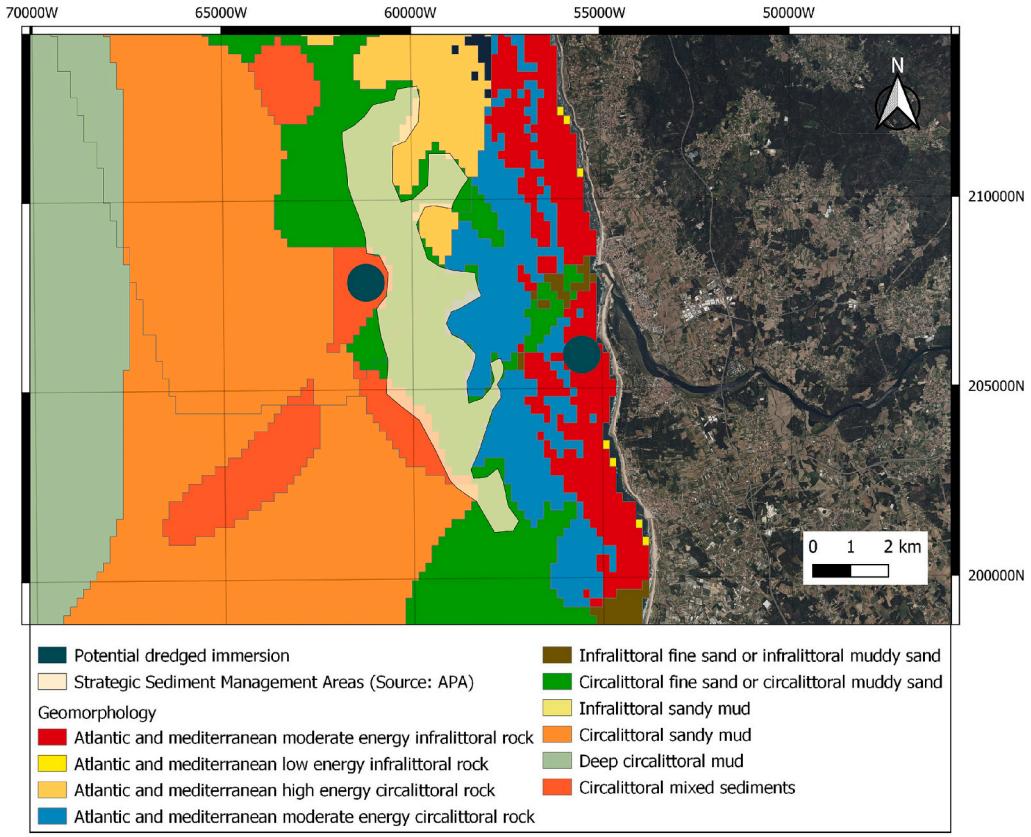

Fig. 3. – Geomorphology, dredging sites and sedimentary areas of interest at Esposende.

offshore region provides more opportunities, from a standalone energy perspective, a nearshore solution is required for the Esposende case study. Therefore, an OWSC technology is proposed [53,54]:

i. The nearshore operational range of OWSCs, like the WaveRoller®, is situated at 8 to 20 m water depth [55], about 1 to 2 nautical miles away from the Esposende shoreline;
ii. Having a single mobile element that is mostly or fully submerged, an OWSC has virtually negligible visual impact;
iii. The rated power tends to be relatively high, at 1 MW or more for utility-scale variants, which enables a high amount of wave energy conversion – estimated capacity factor CF of 0.25 to 0.50 for the WaveRoller® [55];
iv. Sea trials and numerical study, with SNL-SWAN, on the WaveRoller® device at Peniche, Portugal, have been conducted recently,

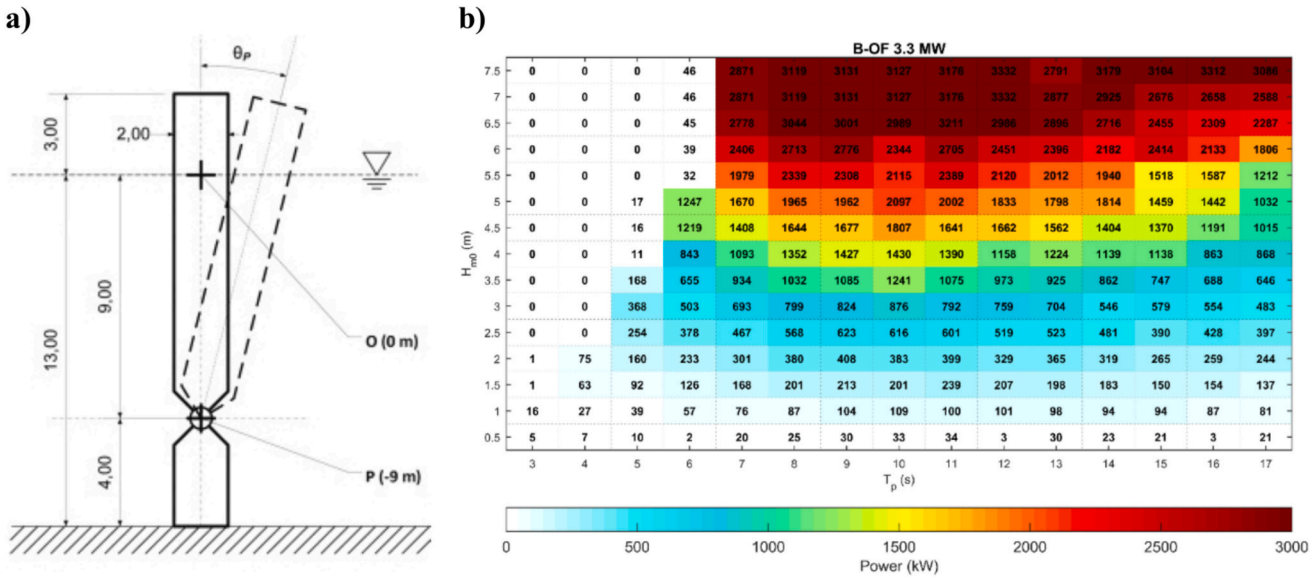

Fig. 4. – (a) OWSC/B-OF representation, from the seabed (−13.0 m from waterline) to the emerged paddle section (+3.00 m from waterline), and (b) power matrix, in kW, with the significant wave height represented in spectral format H_{m0}. Adapted from [54] and [44], copyright 2012 and 2022, elsevier.

with useful information being available in literature [16,40]. Moreover, this study provides novel considerations like handling marine space restrictions, as addressed in Section 2.5.

OWSCs operate through wave-induced surge motions of a submerged panel/flap about a hinged connection, near the seabed foundation. This cyclic motion drives hydraulic pistons to pump high-pressure fluids to a hydraulic motor that drives an electric generator, from which electricity is sent to the mainland grid through subsea cables [54]. For this study, a representative OWSC – Bottom-fixed Oscillating Flap (B-OF) – was considered, as done in literature [15,54]. A visual representation and power matrix are provided in Fig. 4. The B-OF is 26 m wide parallel to the wave front, 2 m thick and 16 m high, 14 m of which for the paddle.

2.5. Marine space conflicts and additional restrictions

Upon deployment at sea, the proposed WEC farm will face numerous marine space conflicts with other activities, from fishing to protected areas. To minimize these occurrences and provide a more realistic scenario, the main marine space restrictions within the case study region are, hereafter, listed and discussed.

2.5.1. Protected areas and natural habitats

The Esposende nearshore is integrated into the Natura 2000 Network [56] – reference PTCON0017, Littoral North Natural Park (LNNP). Rocky outcrops, classified as a Special Conservation Zone, serve as reefs for benthic communities, mostly mainly near the shoreline. The dune system is equally important for local *fauna* and *flora*. There are also biogenic reefs near the Western LNNP, made up of sand mixed with seashells from marine molluscs [57].

The LNNP marine area is subjected to significant pressure, such as coastal erosion attributed to local wave conditions and anthropogenic activities (e.g., tourism, nautical activities, and fishing). Implementing a WEC farm may seem contradictory, but there is more to it. First, this would not be the first time that an OWSC was deployed at sea, in Portugal, within the framework of the Natura 2000 network [58,59]. Second, the farm proposal avoids, as much as possible, the most sensitive areas. Third, it can serve as an alternative/complement to the coastal protection solution from [46], which would equally imply major works in the protected area. Fourth, the farm's implementation project would have to comply with existing legislation and undergo an environmental impact assessment study. Mitigation measures and cost-benefit analysis would have to be implemented alongside a favourable decision from local stakeholders. This is equally valid for virtually any similar proposal, including offshore renewable energy areas [19].

2.5.2. Fishing, tourism, and recreational activities

The marine area of Esposende is of utmost interest to local communities, which include fishermen, surfers, and tourism entities. Fishermen have reported a continuous degradation of accessibility and safety conditions, especially due to sudden accretion combined with the tidal level range and significant sediment flow, which can disable fishing vessels due to insufficient water depth [57]. This causes hazards such as beaching or shipwrecks, forcing fishermen to seek safer conditions at Viana do Castelo. Prevailing arts occur mainly within 3 nautical miles off the coast [50,52]. Tourism and recreational activities are mainly centred at the beaches, which, as seen previously, ought to be conserved.

Implementing a WEC farm may stimulate safer conditions for fishermen, attenuate the erosion of the beach areas, or even provide shelter and energy to promising "blue economy" markets [8,60]. Nonetheless, it would require appreciation from local fishing and tourism authorities to avoid potential conflicts of interest.

2.6. Proposal for compatible farm deployment zones

Accounting for the previous restrictions and considerations, a proposal for an OWSC concept farm is depicted in Fig. 5.

It also features a nearshore projection line (3.0 km long, 300 m away from the shore – 10 %) for evaluating the local influence of the WEC farm (see Section 3.4). It features 150 B-OF units, each rated at 3.332 MW (based on the power matrix and literature [44]), evenly divided into two parks – Farm 1 and Farm 2 (combination designated as Farm 1,2). The total capacity – 500 MW – is in line with recommendations from Laboratório Nacional de Energia e Geologia I.P. (LNEG) [61] for a B-OF device. Their positioning and extension attend to water depth operational range and avoids the main protected areas (shoreline rocky reefs/outcrops and Western biogenic reefs), touristic beaches, sedimentary regions of interest (sand and gravel) and the steeper areas at the 15–10 m depth transition. Placed near the 20 m line, the visual impact is mitigated, given the degree of submergence. The farm's orientation, in accordance with the prevailing wave direction (NW-W), prompts a leeward wave climate attenuation (or wake effect) towards the river mouth and Ofir sandspit, thus promoting safer conditions to other activities.

From this baseline proposal, the study focuses, hereafter, on evaluating the WEC parks' performance by adjusting the farm's orientation, configuration, layout spacing, and generator rating. Based on existing literature [39,62,63], the parks should be oriented approximately parallel to the incoming wave front, and apply inter-device spacing as (sub-) multiples of the characteristic width D (unitary as default, or 26 m). On the configuration, common setups include staggered – henceforth designated as "W" –, aligned – "III" – or delta – "A" shape. However, given the characteristics of the case study area, only the "W" and "III" were deemed adequate. The "A" alternative, by contrast, would imply either a larger deployment area or a reduced number of WECs. To these main study variables add those related to the representative sea-states and tidal levels. Both are addressed next, alongside the formulation and setup of the SNL-SWAN code.

3. Theoretical formulation for the numerical model

In this section, the employed methodologies regarding the representative sea-state triage (statistical K-Means procedure), the underlying premises and inner workings of the SNL-SWAN code, and the main simulation plan are provided, in this order. This enables a better understanding of the theoretical premises for adequately applying such procedures, as well as the convergence studies and numerical settings employed at this stage of the study.

3.1. Wave propagation model overview

For simulating wave evolution over variable bathymetries, two distinct modelling approaches are commonly used. On the one hand, deterministic or phase-resolving models, which directly solve the Navier-Stokes or Euler equations, or their simplified counterparts, like the Reynolds-Averaged Navier-Stokes (RANS) equations and linear Potential Flow Theory. These models provide a detailed representation of individual wave evolution, considering various physical processes that influence their dynamics. In contrast, phase-averaging models do not resolve the evolution of the individual waves but describe the spatial and temporal variation of statistical wave properties, such as the wave spectrum. However, when it comes to wave energy-related studies, such as resource characterization and assessing WEC far-field impacts, phase-averaging wave models appear to be the most common option. This is justified by their simplicity of implementation and computational efficiency when compared to phase-resolving models.

Among the wide range of phase-averaging models utilized in wave energy applications, the open-source third-generation SWAN model stands out as a major option [36]. SWAN simulates wave propagation, considering different wave transformation processes, by solving the wave action balance equation:

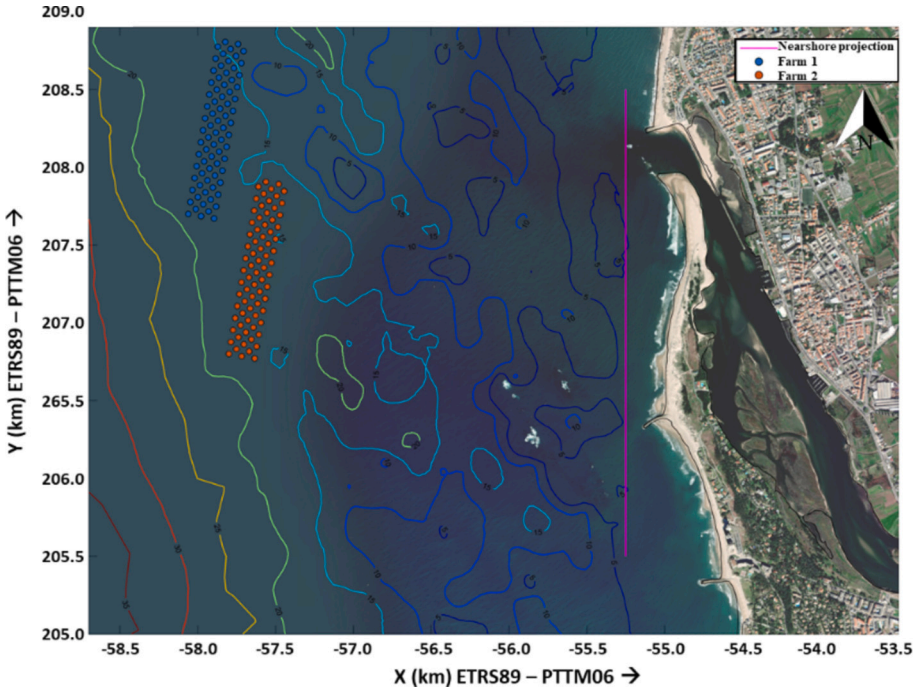

Fig. 5. – Baseline WEC farm proposal for nearshore Esposende. Approximate coordinates, in km, of the 1st unit for: farm 1 (−58.06, 207.70) and farm 2 (−57.80, 206.80) – ETRS89 / Portugal TM06 coordinate system. Default orientation of approximately 280°, 1 D spacing, "W" configuration.

$$\frac{\partial N}{\partial t}+\nabla\left(\vec{C}N\right)+\frac{\partial c_\sigma N}{\partial \sigma}+\frac{\partial c_\theta N}{\partial \theta}=\frac{S_{tot}}{\sigma}, \tag{1}$$

where $\vec{c}$ denotes the propagation velocity in the geographical space, σ and θ represent respectively the relative frequency and direction of waves, while c_σ and c_θ correspond to the propagation velocities in the spectral σ and θ space. N stands for the wave action density, which is defined as the variance density spectrum $E(\sigma,\theta)$ divided by the relative frequency:

$$N(\sigma,\theta)=\frac{E(\sigma,\theta)}{\sigma}, \tag{2}$$

The right-hand side of Eq. 1 represents the source and sink terms, encompassing various physical processes such as generation, dissipation, and non-linear wave-wave interactions:

$$S_{tot}=S_{in}+S_{nl3}+S_{nl4}+S_{ds,w}+S_{ds,b}+S_{ds,br}, \tag{3}$$

where S_{in} is the wave growth by wind; S_{nl3} and S_{nl4} refer to the non-linear transfer of wave energy through three-wave (triads) and four-wave (quadruplets) interactions, respectively; $S_{ds,w}$, $S_{ds,b}$ and $S_{ds,br}$ represent the wave decay due to whitecapping, bottom friction and depth-induced wave breaking, respectively.

Finally, from the full wave spectrum $E(\sigma,\theta)$, SWAN is able to compute the components of wave power per meter of wave front (J_x and J_y), based on Eqs. 4 and 5:

$$J_x=\rho g\int_0^{2\pi}\int_0^{\infty}c_g(\sigma,d)E(\sigma,\theta)cos\theta \mathrm{d}\sigma \mathrm{d}\theta, \tag{4}$$

$$J_y=\rho g\int_0^{2\pi}\int_0^{\infty}c_g(\sigma,d)E(\sigma,\theta)sin\theta \mathrm{d}\sigma \mathrm{d}\theta, \tag{5}$$

where ρ is the water density, g is the gravity acceleration, c_g represents the group velocity, while x and y are the grid coordinate directions. Therefore, the wave power per meter of wave front, J is calculated as:

$$J=\sqrt{J_x^2+J_y^2}. \tag{6}$$

On these grounds, SWAN has been successfully applied for wave resource characterization for a wide range of wave climates and coastal areas [64–66], to which adds initial estimates of far-field impacts of wave energy farms on the wave climate. To achieve this goal, WECs are simulated as porous obstacles crossing at least two grid cells, which act as energy sinks in the wave action balance equation (Eq. 1), extracting a fraction of the incident wave energy [67]. Therefore, the WEC energy absorption is governed by a transmission coefficient, K_t, which represents the ratio between the transferred and incoming H_s. However, this approach has notable limitations, as it results in a constant energy absorption from each incident wave period, whereas, in reality, it depends on both the wave period and wave height. Despite these limitations, numerous studies have embraced this approach to evaluate how well wave energy farms perform in mitigating severe wave conditions, even within co-located offshore wind energy farms and coastal regions [30,68,69]. For that purpose, K_t was empirically defined based on the WEC characteristics [67].

3.2. SNL-SWAN formulation remarks

To overcome the shortcomings of SWAN in modelling WECs' energy absorption, researchers at the Sandia National Laboratory developed the so-called SNL-SWAN [42]. It introduces new formulations into the source code of SWAN to compute the obstacles' K_t, based on WEC absorbed power (either the WEC power matrix or the relative capture width ratio – CWR – curve [70]). In addition, SNL-SWAN allows for the K_t to be calculated as either a constant value, applicable to all frequencies, or as a frequency-dependent value [45], enabling the K_t adjustment in response to varying wave conditions across both temporal and geographical spans. With the B-OF power matrix being available, and given the greater accuracy of the frequency-dependent approach [23], the OBCASE3 was employed to compute K_t in this study.

In SNL-SWAN, WECs are treated as line obstacles with the same width as the device, and the model only accounts for them when they intersect with the grid. Therefore, to ensure accurate modelling of WEC energy absorption, it is crucial to select a computational grid size that ensures the WEC obstacle crosses at least 5–6 grid cells, as recently

evaluated in [23]. It is worth pointing out that SNL-SWAN has been verified and preliminarily validated against experimental data [43,71,72]. In consequence, SNL-SWAN offers a higher degree of accuracy in assessing the energy absorption of WECs and their impacts on the far-field wave climate when compared to the original SWAN code. This is reinforced through adequate model setup.

3.3. Numerical model setup

Initially, a regional SWAN model successfully implemented/validated in [46,73] was used to obtain data on local wave conditions, at Esposende. To capture the seasonal wave climate variations, the model was run for a 31-year period (1990 to 2020) with a one-hour frequency interval, resulting in over 270,000 sea-states (see Section 2.2 and Fig. 2). After, given the significant number of sea-states, a statistical K-Means clustering approach was employed to define a set of representative wave conditions (see Section 3.4).

Moreover, SNL-SWAN was employed to evaluate the performance of various wave farm configurations, focusing on both wave energy and coastal protection metrics. The model was implemented in a Cartesian grid, as described in Table 2. This setup conserved the listed parameters and retained the core of the validated model from the Ofir sandspit study [46]. However, with the introduction of the WEC farm, it was necessary to adjust the grid resolution according to literature recommendations of grid cell intersections per WEC unit. A preliminary grid convergence study is discussed in the next sub-section. The bathymetric dataset was obtained from Navionics (offshore and nearshore), Polis Litoral Norte (river mouth) and Programa COSMO (topography). It was then subjected to triangular interpolation, followed by internal diffusion, onto the computational grid, using the Delft3D-QUICKIN toolbox [74]. This ensured adequate aspect ratio, Courant number and orthogonality values towards high-fidelity simulations [36,37].

3.4. Sea-state selection, grid convergence and simulation plan

The K-Means approach involves systematic partitioning of n data points into a specific number of K clusters. The unique data ought to share a significant degree of similarity within each cluster, but clusters should differ from one another. This is evaluated iteratively by minimizing the squared Euclidean distance *SED*, or sum of square errors, between the data points and the cluster's centroid, which is updated until a convergence criterion is met:

$$SDE = \sum_{k=1}^{K} \sum_{m_i \in M_k} \|m_i - \mu_k\|^2 \tag{7}$$

where m_i is a data member, M_k the set of members found in cluster k, and μ_k the vector mean of cluster k. The latter is a function of the number of members in M_k, ε_k, being defined as:

$$\mu_k = \frac{\sum_{m_i \in M_k} m_i}{\varepsilon_k} \tag{8}$$

K-Means provides a computationally efficient tool that, unlike the binning methodology [75], can fully incorporate and condense a large dataset into a limited number of representative sub-groups (sea-states, in this study) [76]. To put it into perspective, simulating all 270,000 sea-states with multi-variable analysis would require over one year of uninterrupted simulations with a High-Performance Computer (HPC) – over 20,000 CPU cores, 2.2 GHz and up to 4 PetaFLOPS (including GPUs). Furthermore, K-Means was successfully employed in other studies on wave energy conversion and representative sea-state selection [76,77]. However, it is worth noting that K-Means only ensures a local optimum that may depend on the centroid initialization, and its distance-based nature warrants data standardization.

In this study, distinct combinations of cluster number, centroid iteration and data standardization were evaluated. For comparison, the metric proposed in [76] was used, which is very similar to the well-known Mean Absolute Percentage Error *MAPE*. Henceforth, it will be designated as such:

$$MAPE = \frac{1}{n} \sum_{i=1}^{n} \left| \frac{x_i - x_i^*}{x_i} \right| * 100 \tag{9}$$

where x_i and x_i^* are the real/measured and estimated values, respectively.

Considering the recommendations found in [76], a range of 5 to 15 clusters was initially considered. This was done with IBM® SPSS® Statistics, a robust statistical analysis software [78]. Data standardization included an in-built option from SPSS®, data compression to a range between 0 and 1 (min-max range), and two distinct ratio-based alternatives: data split by the corresponding variable mean (1.99 m, 10.47 s and 294.30°) or median (1.74 m, 10.31 s and 298.00°). Given the large number of simulations, only the most relevant outcomes are discussed (i.e., the ones with statistical significance, p-value <0.05). In detail, a tighter cluster range between 5 and 8 for the 0–1, mean and median standardizations provided the lowest *MAPE* on the three sea-state variables. This metric was also computed for the wave power resource, J, assuming deep water conditions. Note that J was not directly considered for the clustering procedure, but rather calculated based on the H_s and T_p results (deep water formula).

MAPE results are summarized in Table 3 to Table 5. Overall, the 0–1 clustering and 6 clusters tended to yield higher *MAPE* values, mainly for J and H_s. This was mainly due to limited variability of T_p and *Dir,* which was also observed for 5 clusters. In contrast, the dataset included specific occurrences of interest, such as incoming waves from non-NW-W octants and "storm" conditions characterized by relatively large $H_s - T_p$ values. These were better identified through the mean and median approaches, mainly with 7 or 8 clusters. They generally exhibited an encompassing representation of prevalent $H_s - T_p$ values whilst yielding lower *MAPE*, of similar magnitudes to those in [76,77]. Overall, the median approach with 8 clusters tended to provide slightly more representative sea-states with relatively lower *MAPE*s, at an adequate convergence rate (15

Table 3
– Clustering *MAPE*: 0–1 standardization.

N° clusters	Variable *MAPE* (%)			
	J	H_s	T_p	*Dir*
5	107.72	33.04	11.80	5.28
6	128.40	103.20	22.10	4.90
7	96.09	30.39	9.77	5.72
8	97.58	31.45	9.43	5.31

Table 2
– Numerical model setup parameters.

Grid extension (km)		Spectral resolution		Frequency interval		
Longshore(x or M)	*Cross-shore(y or N)*	*Type(–)*	*N° directions(–)*	*Lowest(Hz)*	*Highest(Hz)*	*N° frequency bins(–)*
3.90	3.75	Circle	36	0.05	1	24
Depth-induced breaking		**Bottom friction**		**Wave propagation processes**		
Alpha(–)	*Gamma(–)*	*Type(–)*	*Coefficient(m^2s^{-3})*	*Whitecapping(–)*	*Refraction(–)*	*Frequency shift(–)*
1.00	0.73	JONSWAP	0.067	Komen et al. *(1984)*	Active	Active

Table 4
– Clustering *MAPE*: mean value standardization.

N° clusters	Variable *MAPE* (%)			
	J	H_s	T_p	*Dir*
5	46.85	17.24	15.86	3.30
6	59.72	99.14	26.04	3.00
7	48.90	17.08	15.54	6.92
8	47.81	16.67	15.53	6.68

Table 5
– Clustering *MAPE*: median value standardization.

N° clusters	Variable *MAPE* (%)			
	J	H_s	T_p	*Dir*
5	46.15	16.83	16.56	3.60
6	57.24	96.44	26.04	3.30
7	47.80	16.84	16.04	7.19
8	45.70	15.55	15.91	6.94

iterations or less, controlled automatically by the SPSS software). More clusters would cause greater partition of intermediate sea-states, implying additional simulations effort for similar *MAPE*s. Hence, the selected clustering option was 8, Fig. 6.

From cluster 1 to 8, the data percentages are 1.62 %, 19.60 %, 6.34 %, 11.63 %, 0.81 %, 3.19 %, 29.78 % and 27.02 %. Note that, on the aforementioned occurrences of interest, cluster 1 could be a potential outlier from a practical perspective, considering its representativeness and the $H_s - T_p - Dir$ distribution of Fig. 2. However, cluster 5 also has a very low number of occurrences, yet it can represent severe wave climates. Additionally, from a research perspective, including cluster 1 enables a better understanding of eccentric *Dir* values on the WEC farm's performance. Even if cluster 1 has a negligible impact in this work, the computed patterns could be of interest for similar studies in which such occurrences are pertinent.

Regarding grid convergence, distinct resolutions were simulated for a smaller batch of 30 B-OFs (three rows of 10 units each, based on the default Farm 1 setup). The *MSL* and mean H_s, T_p and *Dir* from the original dataset were considered as wave propagation conditions across the N, W and S boundaries: 1.99 m, 10.47 s and 294.30° (boundaries conserved for the remaining simulations). The absorbed power was individually evaluated for grid resolutions ranging from 7×7 m^2 to 3×3 m^2 (coarser to denser), until a general variability below a 10 % threshold was obtained (i.e., until none of the 30 B-OFs yielded an absorbed power variation of ±10 % or more, from one resolution onto the next). This condition would be met only with a resolution of 3×3 m^2, ranging between an absolute maximum and minimum of 9.9 % and 0.3 % (mean of 4.23 %). Higher resolutions (e.g., 2×2 m^2) would lead to excessively long computational times and memory allocation problems, even in the HPC. Hence, a 3×3 m^2 cell size was selected, resulting in 1250 and 1300 cells in the cross-shore and longshore directions, respectively. Convergence analysis values can be consulted in Appendix A.

Based on approaches found in literature [41,76,79] and the characteristics of this study, the following simulation plan variables were defined:

- Eight representative sea-states with distinct H_s, T_p and *Dir*, including five water/tidal levels (see Table 1). Because there is a noteworthy tide amplitude (over 4 m), not only does the submergence of the B-OFs vary considerably, but the local wave conditions may be affected, given the proximity to the shoreline (shallow waters);
- Three park options – Farm 1 (75 units, Fig. 5 blue lines only), Farm 2 (75 units, Fig. 5 red lines only) and combined (Farm 1,2–150 units, Fig. 5 red and blue lines);

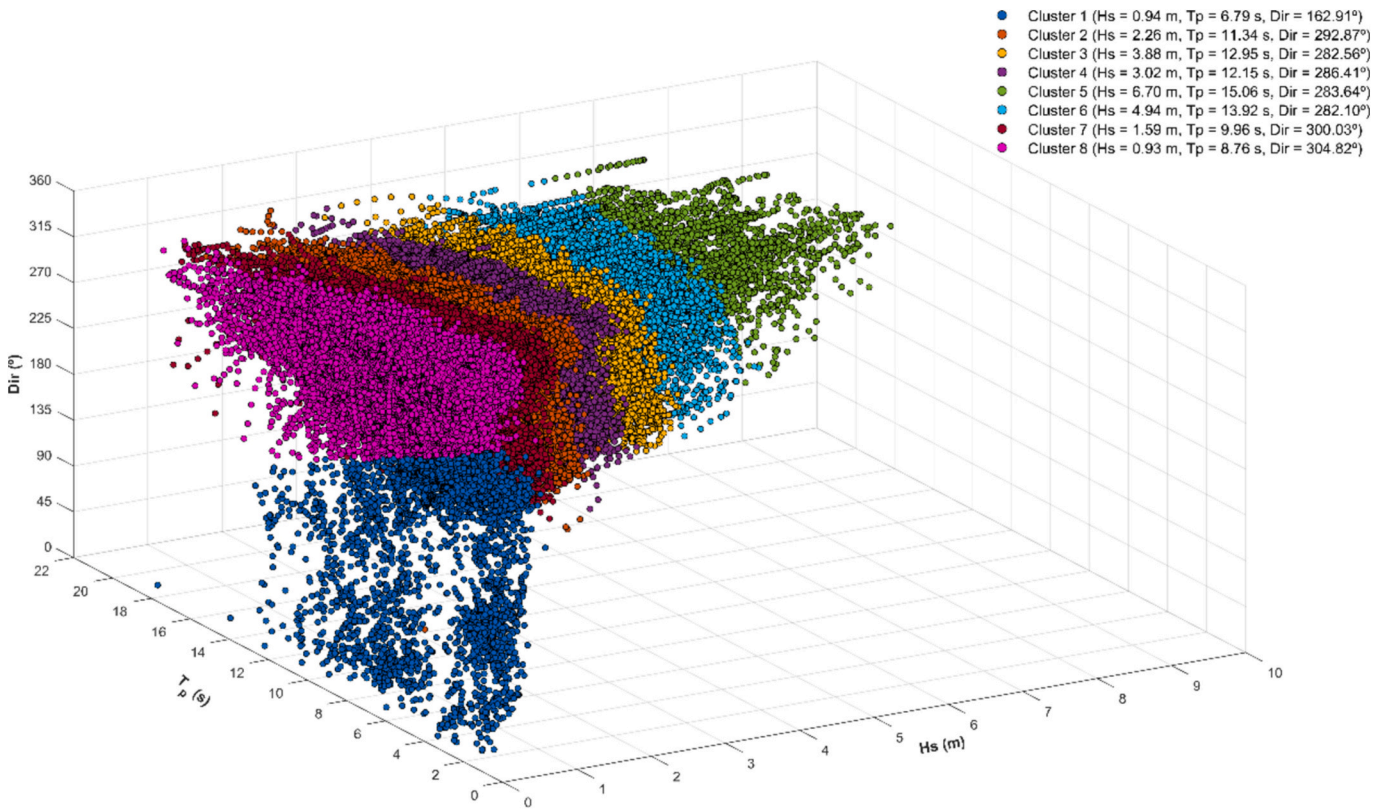

Fig. 6. – Selected clustering solution: 8 representative sea-states with respective centroids.

- Three farm orientations, closely aligned with the prevailing wave front. Given the variability of *Dir* for the eight sea-states, the orientation range was set to about 295 ± 15° (average value ±10 %);
- Two configurations – staggered units (W) pattern and aligned (III) pattern, with five rows of fifteen units each per park;
- Three unit distancing layouts – 1 D, 1.25 D and 1.5 D, which avoids worst-case scenario collisions between the rotating flaps of the B-OFs (<1 D) and either inadequate operational depth ranges or conflict with marine space restrictions (>1.5 D);
- Three distinct generator ratings – 3.332 MW (original from generic B-OF), 2.5 MW (scaled from B-OF power matrix through the Froude-based methodology in [79,80]) and 1 MW (standard commercial WaveRoller®);

The main simulation plan involved distinct variable combinations – 424 runs –, aimed at finding an improved solution for the OWSC/B-OF farm. To these add preliminary simulations for standalone units required for the *q*-factor, Fig. 7. The CF and *q*-factor metrics, which are standard in this type of study for evaluating WEC efficiency and constructive/destructive near-field influence [34], were defined as:

$$CF = \frac{P_{abs}}{P_{rated}} \tag{10}$$

$$q-factor = \frac{\sum_{i=1}^{n} P_{abs,i}}{\sum_{i=1}^{n} P_{stdalone,i}} \tag{11}$$

where P_{abs}, $P_{stdalone}$ and P_{rated} are, respectively, the absorbed power of a WEC park unit, of a standalone unit (no park effect) and its power rating. Note that a *q*-factor above 1 implies constructive interference (i.e., the interference patterns between the farm units and the surrounding wave field allows to generate more power than the cumulative output of standalone isolated units). Destructive interference is associated with a *q*-factor below 1 (i.e., the farm's power output is lower than the cumulative output of the same number of standalone isolated units). Hence, a destructive interference is undesired, as it implies a reduction of the effective capacity of the WEC farm. By contrast, a constructive interference pattern can enhance the overall power output without adding more units.

On the evaluation of coastal protection, a Variability Index, *VI*, was selected. Using H_s as the reference variable, this index can be defined as:

$$VI(\%) = \frac{\left(H_{s,with\ WECs} - H_{s,no\ WECs}\right)}{H_{s,no\ WECs}} \tag{12}$$

By default, *VI* is negative if the considered variable is reduced (e.g., H_s attenuation due to the WEC park). Lastly, since SNL-SWAN provides the individual WEC power outputs, the absorbed energy can be estimated by multiplying these outputs by the operation time per cluster. On a standard year of 8760 h and neglecting availability and generator efficiency, the Annual Energy Production *AEP* can be estimated as:

$$AEP = \sum_{i=1}^{8} \sum_{j=1}^{n} P_{abs,ij} h_i, where\ n = 75\ or\ 150\ (one\ or\ both\ farms) \tag{13}$$

where h_i is the number of operational time hours associated with cluster *i*.

4. Results

Following the stepwise evaluation from Fig. 7, the first stage involved the definition of the parks' orientation towards the waves. Note that the 280°, 295° and 310° regard, as a reference, the incoming waves' direction, with the two parks being always perpendicular to them (see Fig. 5).

4.1. Park orientation selection

From Fig. 8 and Table 6, it is perceivable that clusters 2 to 4 are the main contributors to the *AEP* in all cases. This is attributed to a combination of i) cluster centroids overlapping with "hot-spots" in the B-OF power matrix, ii) number of cluster data points, iii) and the associated

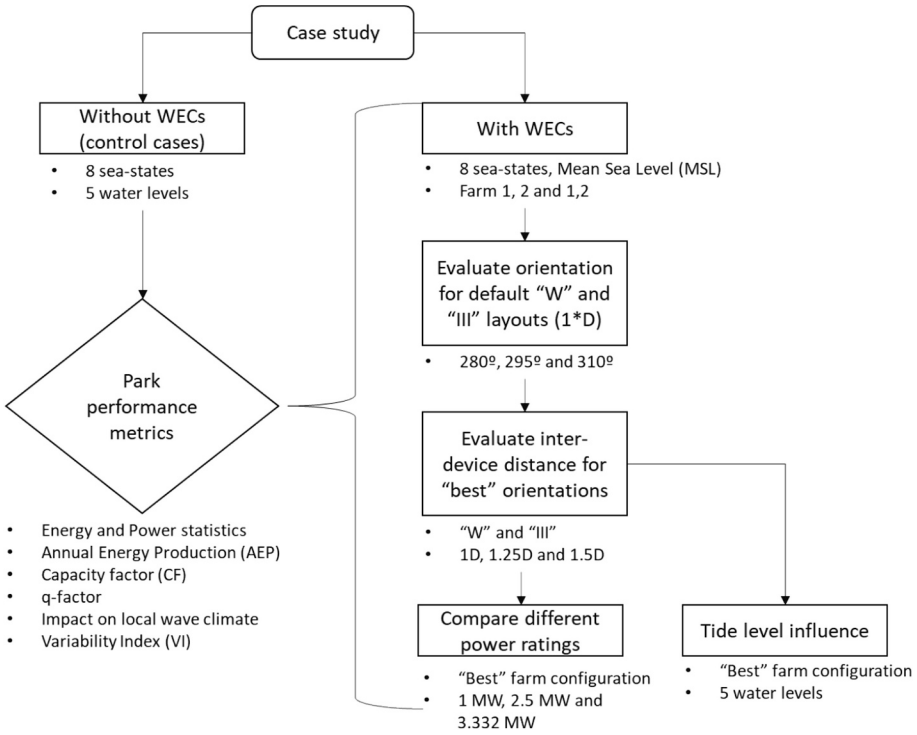

Fig. 7. – Flowchart of the simulation plan for the Esposende case study.

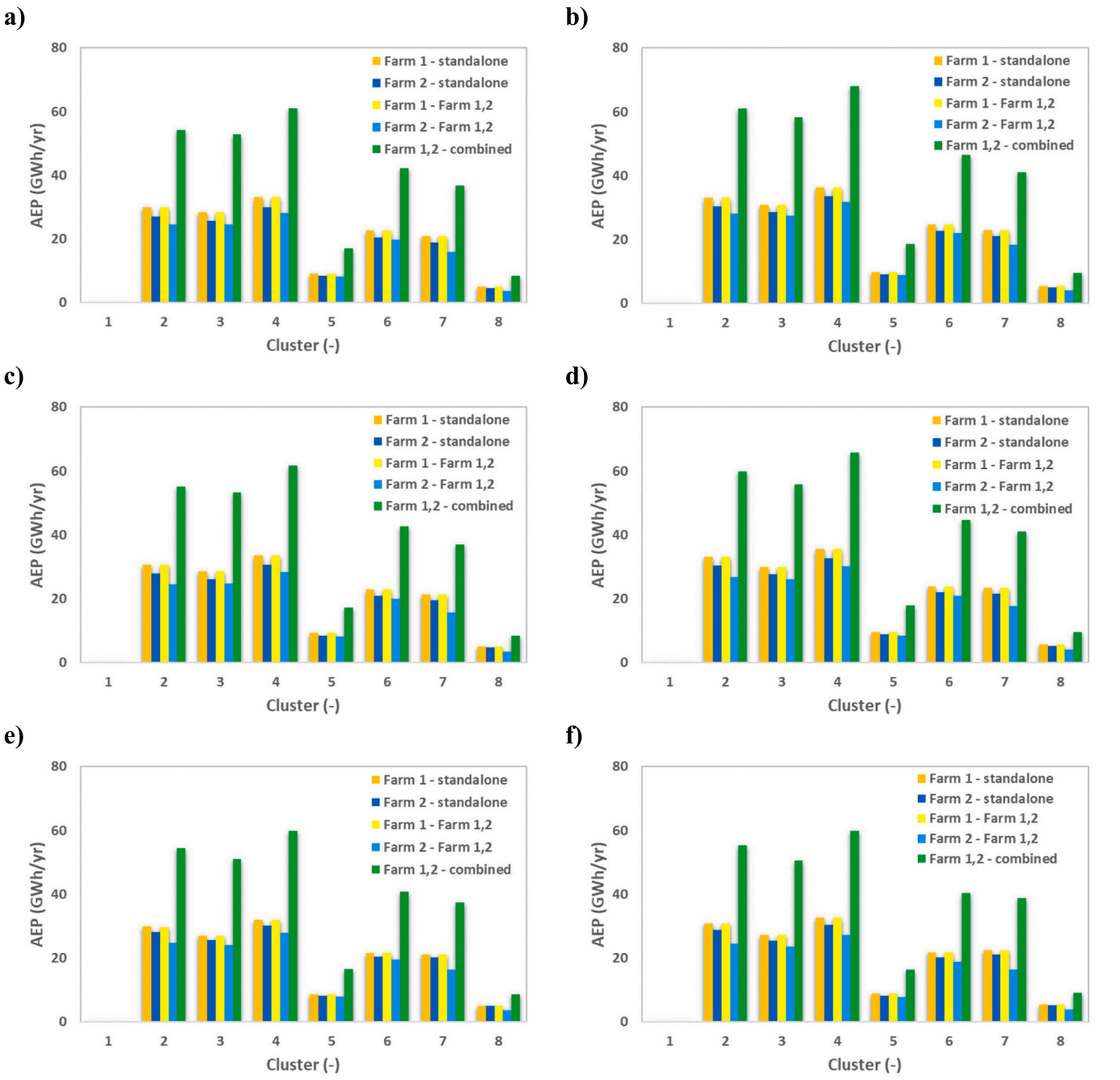

Fig. 8. – *AEP* per park and cluster for a) III 280°, b) W 280°, c) III 295°, d) W 295°, e) III 310° and f) W 310°.

$H_s - T_p - Dir$. Cluster 8, for instance, has far more data points than cluster 4, but the wave conditions are more beneficial for cluster 4 (e.g., higher $H_s - T_p$ implies a greater J, and the centroid overlaps an area of the power matrix with higher absorption values). Cluster 1 is similar to cluster 8, but the *Dir* and number of data points are far less favourable, causing cluster 1 to have a negligible impact on the *AEP*.

The "W" configuration tends to yield better energy absorption results than "III" for all cases, due to a stronger inter-row "shadowing" effect in "III". Absorbed power reduction percentages range from −46.13 % to −98.20 %, which tend to be inversely proportional to H_s. Additionally, for cluster 4, the standalone Farm 1 absorbs, in total, about 0.03 % more than the Farm 1,2 counterpart, while greater differences are observed between the standalone Farm 2 and its counterpart in Farm 1,2.

Regarding farm orientation, Fig. 9, "W" 280° and "III" 295° stood out. Cluster 1 always benefits the 310° orientation, while others tend to yield higher values for "W" 280° and "III" 295°, since the *Dir* values for clusters 2 to 8 vary from 282.10° to 304.82°. Also, the 1st to 2nd row reductions would tend to be proportionally greater for "W" 295° (e.g., 19–20 % and 10–15 % for clusters 4 and 5) than for 280° (e.g., 11–13 % and 3–8 % for clusters 4 and 5). The difference gap is reduced going towards the 5th row, but the pattern is conserved. Similar outcomes were observed for the "III" 280° and 295°, albeit with a lesser reduction discrepancy and with the latter being, in this case, benefited.

On the local impact, there is a substantial reduction of H_s due to the farm's presence, as the B-OF units absorb part of the wave energy (proportional to H_s^2). The wake areas extend up to 2.0 and 2.5 km in the longshore and cross-shore directions, correspondingly. *VI* negative values reach peaks of about −70 % and are slightly higher for "W" 280° and "III" 295°, in line with the *AEP* results.

Table 6
– *AEP* per sea-state cluster for Farm 1,2, under different farm orientations.

Cluster	*AEP* (GWh/yr)								Total
	1	*2*	*3*	*4*	*5*	*6*	*7*	*8*	
III, 280°	0.153	54.288	52.748	61.023	17.065	42.238	36.631	8.362	272.507
W, 280°	0.152	61.012	58.253	68.069	18.512	46.456	41.121	9.364	302.939
III, 295°	0.177	55.008	53.247	61.735	17.244	42.680	37.032	8.404	275.527
W, 295°	0.177	59.750	55.850	65.683	17.914	44.577	40.973	9.510	294.433
III, 310°	0.199	54.468	51.022	59.959	16.447	40.871	37.349	8.596	268.913
W, 310°	0.199	55.258	50.537	59.846	16.343	40.396	38.639	9.087	270.307
1st (waveward) to 5th (leeward) row maximum variation in absorbed power per cluster (%)									
III, 280°	−68.50	−71.87	−62.33	−67.06	−50.72	−59.98	−81.07	−96.16	
W, 280°	−70.32	−71.04	−59.01	−64.98	−46.13	−56.65	−81.98	−98.20	
III, 295°	−83.53	−72.94	−61.99	−67.40	−50.68	−59.91	−80.42	−95.56	
W, 295°	−80.03	−72.82	−60.41	−66.32	−47.69	−57.88	−82.16	−97.29	
III, 310°	−90.86	−72.53	−61.60	−66.92	−48.86	−58.59	−79.28	−95.32	
W, 310°	−93.02	−72.88	−61.50	−66.92	−48.79	−58.58	−81.38	−96.73	

4.2. Park layout evaluation

The two distinct B-OF park locations, in the absence of WECs, were expected to exhibit slightly different wave conditions and energy values from one another. Furthermore, by incorporating the parks, different positions and distancing between WECs would likely prompt distinct wave front conditions reaching the devices, at different depths. To this adds near-field interactions between the B-OF units, and the surrounding wave field. Given the increasing inter-device distancing from 1D to 1.5D, the wake effect was expected to diminish accordingly in the near-field, thus bolstering the energy yield. This was corroborated for all "W" and "III" layouts, Table 7, with 1.5D being the best option for all cases. Note that, henceforth, the definition of "pondered" assumes a weighted contribution per cluster towards the estimated quantity (i.e., each cluster has a contribution equivalent to its percentage of records from the totality of the dataset).

The outcomes are further corroborated by the boxplots in Fig. 10. From 1D to 1.5D there is a general uplift of the boxes' positions, mainly for the leeward rows, as expected from the mitigated "shadowing" effect. There is also an overall greater power variability from 1D to 1.5D, as the B-OFs also extend towards the coastline and shallower waters, which also affects the wave absorption process. Analogous occurrences were reported in [23]. These patterns were identified for all clusters apart from cluster 1, which provided opposite trends due to the distinct *Dir* of the incoming waves (162.91°, from SE to NW).

The *VI* metric was employed at the nearshore projection line (alongshore distance), for all clusters and layouts. Overall, a larger *D* promotes a more effective H_s reduction, as seen from the lower positions of the curves and statistical parameters in Fig. 11 and Fig. 12. The broader area of influence and greater energy absorption contribute towards this outcome, in line with [23]. Note that clusters 6 and 8 are depicted, as they are representative of the curve patterns identified for the remaining clusters (cluster 7 similar to 8, all others similar to 6, apart from 1).

There are significant variations along the nearshore projection line, parallel to the coast, due to the varying bathymetric profile and the combined influence of the two B-OF parks. South of the line (0.0 to 0.5 km), the impact is very limited regardless of inter-device spacing, in agreement with Fig. 9. The *VI* values were generally lower (i.e., negative and with greater magnitude) for the "W" configuration, as expected. The pondered mean for "W" 280° went from −9.98 % (1D) to −11.65 % (1.5D), in contrast to "III" 295's range of −8.60 % to −10.39 %. Pondered peak H_s reductions of −25.54 % and − 22.55 % were reported, correspondingly (entire nearshore line), as well as negative peak values beyond −30 % (punctual). These statistical values consider all clusters and are consistent with the *AEP* trends: with more absorbed energy by the B-OF farm, less wave energy reaches the shoreline, though the wake weakens upon approaching it.

Overall, the "W" 280° 1.5D emerged as the most promising option. A summary on the local wave resource impact is provided in Fig. 13. Again, under distinct sea-states, the two B-OF parks' spacing can have a relevant effect on the local wave conditions and resource, particularly along Ofir's sandspit. Inter-park "shadowing" is stronger in the 1.5D layout, to which adds a clear influence of bathymetric profiles (*e.g*, the aforementioned low-depth areas East of the farms) and the limited wake effect upon reaching the shoreline. Distinct B-OF power ratings/matrices will be addressed in the next sub-section.

4.3. Rated power and power matrix comparison

Given the different ranges and matrix values of the distinct power ratings, an analysis focused on the CF and *AEP* is provided and discussed hereafter, Fig. 14.

The number of B-OFs and their dimensions were conserved. The former is justified by a fairer basis of comparison on local impact and overall efficiency, albeit at the expense of installed capacity for lower power ratings. The latter is attributed to the similar dimensions of the 3.332 MW B-OF and the 1 MW WaveRoller®, which warrant an equivalent consideration for the 2.5 MW variant, though its power matrix was obtained from a Froude scaling-based methodology [79,80].

From the CF and *AEP* in Fig. 15, energy absorption increases with greater rated capacity – 189.2 GWh/yr, 304.7 GWh/yr and 341.4 GWh/yr for 1 MW, 2.5 MW and 3.332 MW, respectively.

Although the *AEP* increased with the rated power, an opposite trend was observed for the CF, mainly due to the lower denominator values. While the curves were somewhat similar to one another, the pondered mean CF increased from 0.078 (3.332 MW) to 0.144 (1 MW). Apart from cluster 5, the magnitudes seemed to be higher for the latter rating.

Lastly, Farm 1,2 generally yielded slightly lower *CF*s than the standalone Farm 1 and Farm 2, albeit with small variations in clusters 5 and 6. Again, this depends upon the "shadowing" effect between the two parks. The distinct absorption patterns also affected the local wave climate differently, with a more effective wave attenuation being observed for the 3.332 MW rating, as expected. Therefore, the original power matrix was maintained for the final stage of this study: tidal level influence.

4.4. Tide level influence

So far, the water elevation was set at +2.00 m (*MSL*), but tidal levels can influence the productivity and local impact of a WEC farm. From an energy and power perspective, there is a continuous, yet minor reduction in the energy absorption with increasing tidal level, Fig. 16, with negligible influence on the local wave conditions. No significant changes

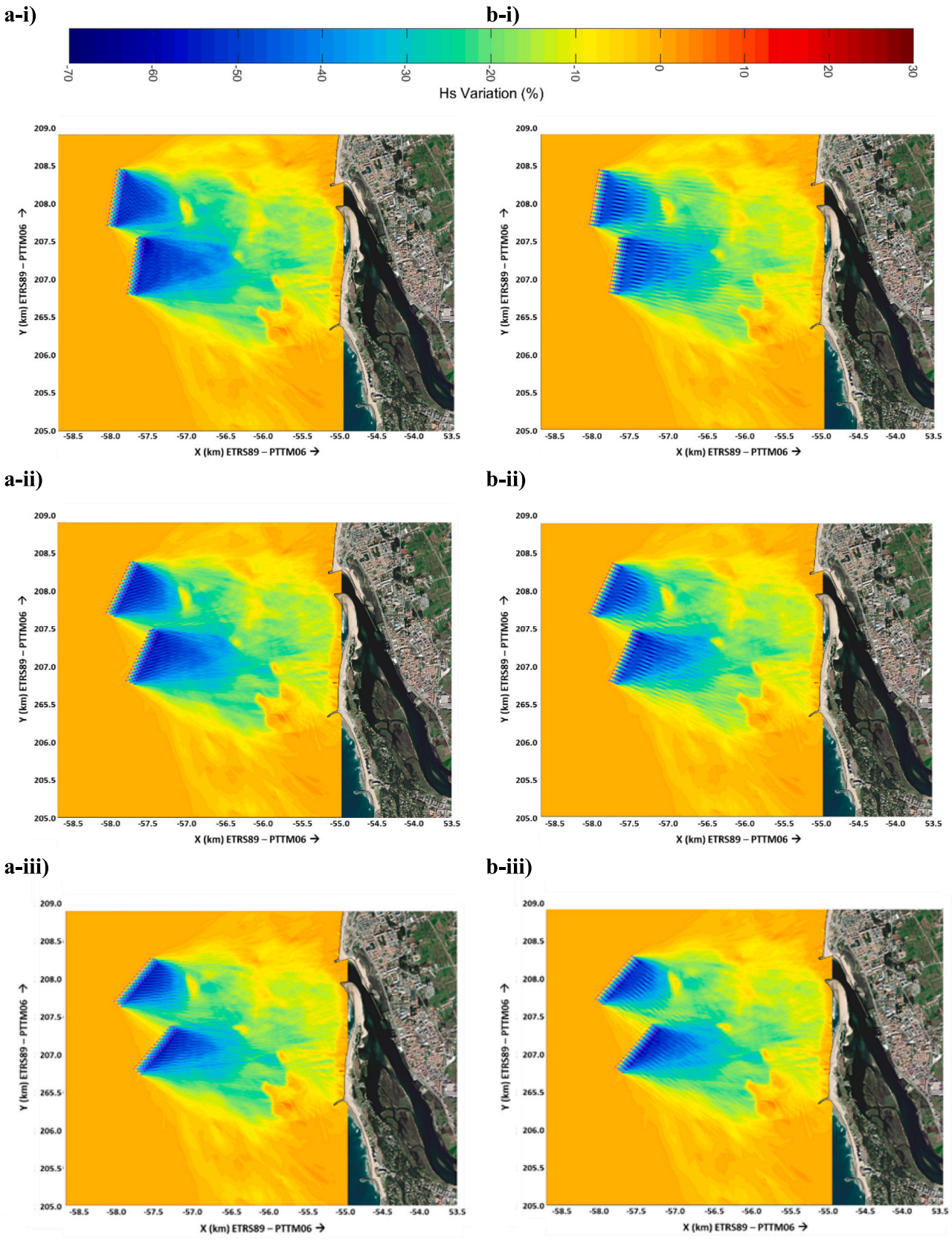

Fig. 9. – Local impact of the B-OF farm, under cluster 4, for distinct orientations and configurations: a-i) "W" 280°, a-ii) "W" 295° and a-iii) "W" 310°; b-i) "III" 280°, b-ii) "III" 295° and b-iii) "III" 310°. The variations are the *VI* metric values for H_s.

Table 7
– *AEP* and *q*-factor per cluster for farm 1,2, under varying park layouts. *q*-factor values in brackets indicate the sum pondered mean values from standalone farm 1 and farm 2, for comparison with the total value of farm 1,2.

	AEP (GWh/yr)								Total
Cluster	*1*	*2*	*3*	*4*	*5*	*6*	*7*	*8*	
III, 1D	0.177	55.008	53.247	61.735	17.244	42.680	37.032	8.404	275.527
W, 1D	0.152	61.012	58.253	68.069	18.512	46.456	41.121	9.364	302.939
III, 1.25D	0.194	59.370	56.572	66.167	17.946	45.216	40.605	9.638	295.707
W, 1.25D	0.169	66.291	62.132	73.364	19.427	49.450	45.330	10.798	326.961
III, 1.5D	0.216	63.976	59.923	70.684	18.510	47.751	44.348	10.942	316.351
W, 1.5D	0.183	69.482	64.320	76.413	19.959	51.147	47.928	11.920	341.353
q-factor (−)									
III, 1D	0.34	0.54	0.64	0.60	0.71	0.66	0.49	0.36	0.49 (0.54)
W, 1D	0.29	0.60	0.70	0.66	0.77	0.72	0.55	0.41	0.55 (0.58)
III, 1.25D	0.37	0.58	0.68	0.64	0.74	0.70	0.54	0.42	0.54 (0.61)
W, 1.25D	0.33	0.65	0.75	0.71	0.81	0.76	0.61	0.47	0.60 (0.67)
III, 1.5D	0.42	0.63	0.72	0.69	0.77	0.74	0.59	0.47	0.59 (0.68)
W, 1.5D	0.35	0.68	0.77	0.74	0.83	0.79	0.64	0.52	0.64 (0.74)

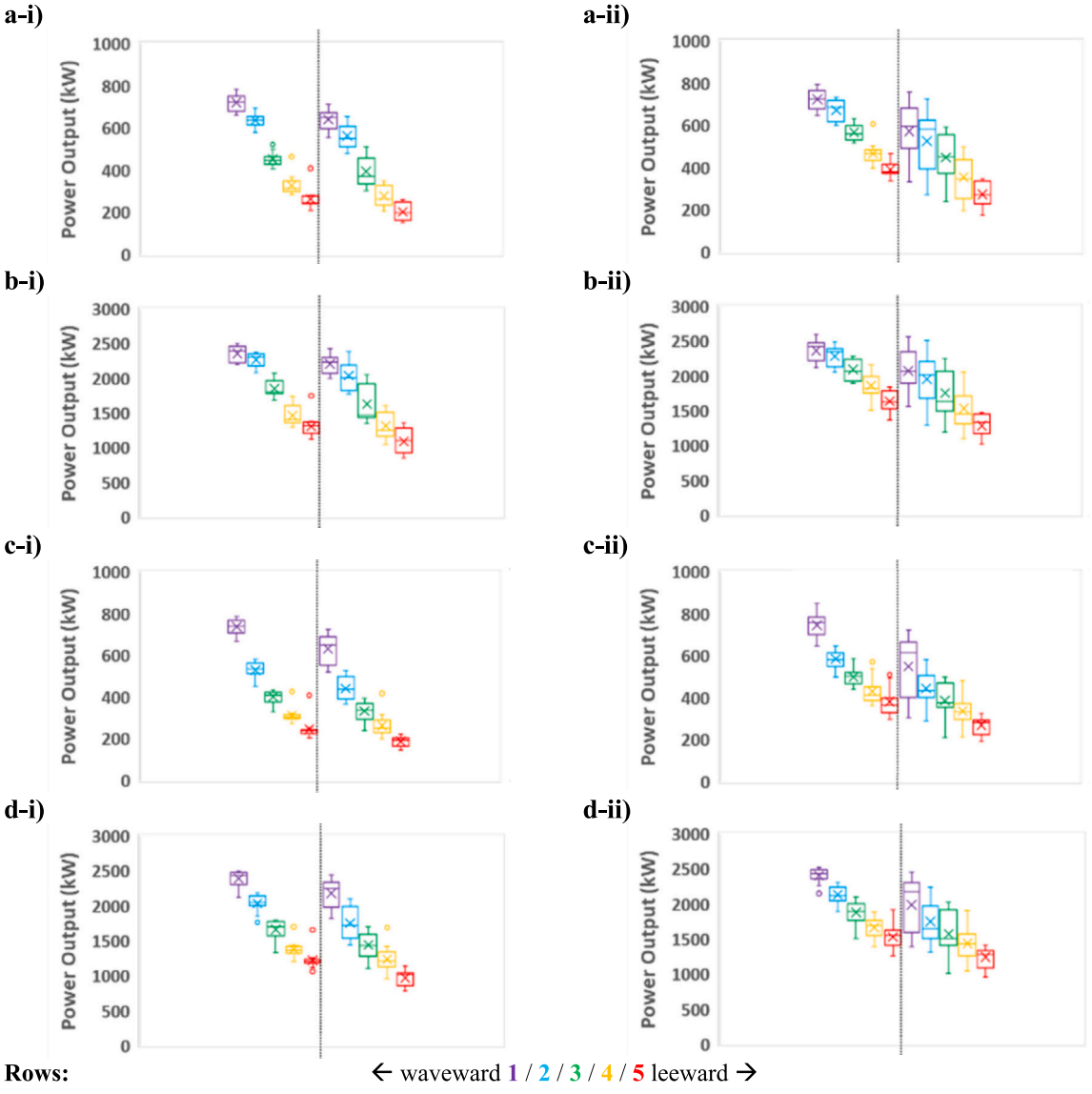

Fig. 10. – Boxplots of B-OF power output for "W" 280° a-i) 1D cluster 4, a-ii) 1.5D cluster 4, b-i) 1D cluster 5, and b-ii) 1.5D cluster 5; and for "III" 295 °c-i) 1D cluster 4, c-ii) 1.5D cluster 4, d-i) 1D cluster 5, and d-ii) 1.5D cluster 5. All plots refer to the combined parks (farm 1,2).

a)

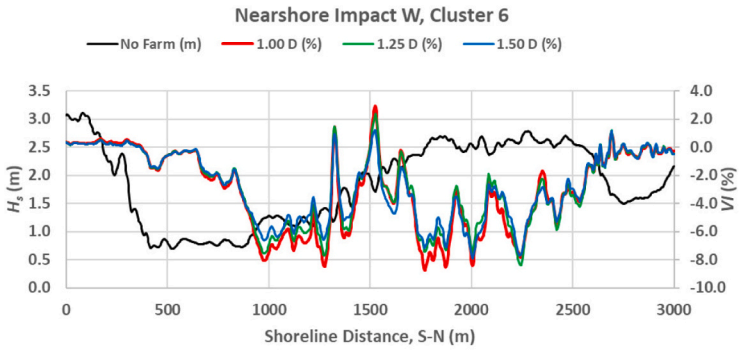

b)

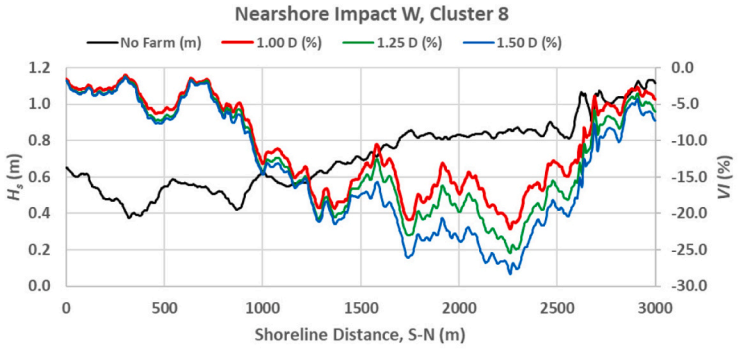

c)

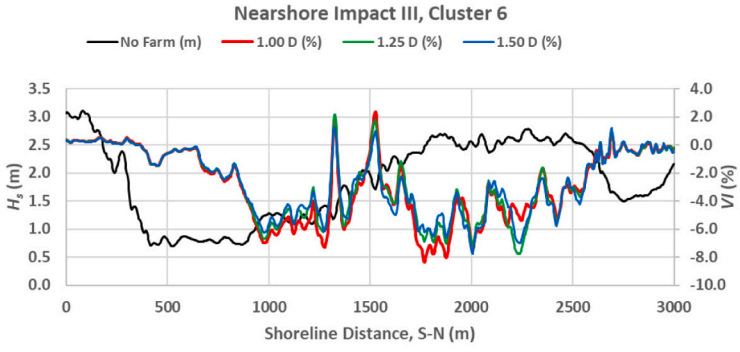

d)

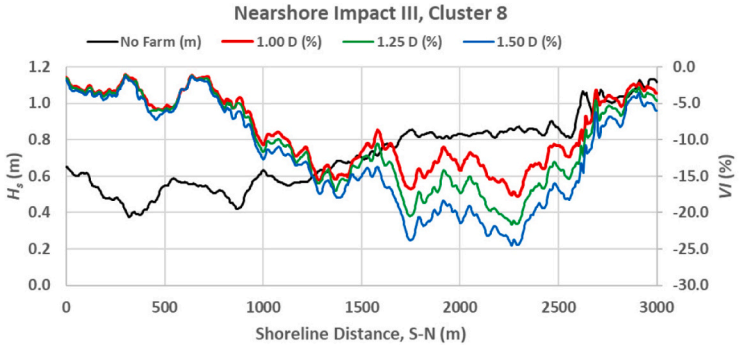

Fig. 11. – Nearshore projection impact of the B-OF farm through the *VI* metric.

were observed against previously identified trends in terms of *q*-factor and CF, but there were exceptions for clusters 1 and 5's *q*-factors. The latter's high $H_s - T_p$ justifies the higher metrics values, while the opposite is observed for cluster 1. Nonetheless, this opposite pattern is not sufficient, alongside the irregular variations of cluster 5's *CF*s, to counteract the generally lower metrics values from the *ZH* to *HT* levels. While all the *q*-factors were below 1, CF values remained somewhat small, apart from cluster 5. This relates to previous remarks on conversion efficiency, as well as the selected B-OF power rating and matrix.

At the nearshore projection line, Fig. 17, important patterns were observed. Firstly, the wave *Dir* clearly influenced the range of the B-OF farm's wake, given the projection of the attenuated region. For instance,

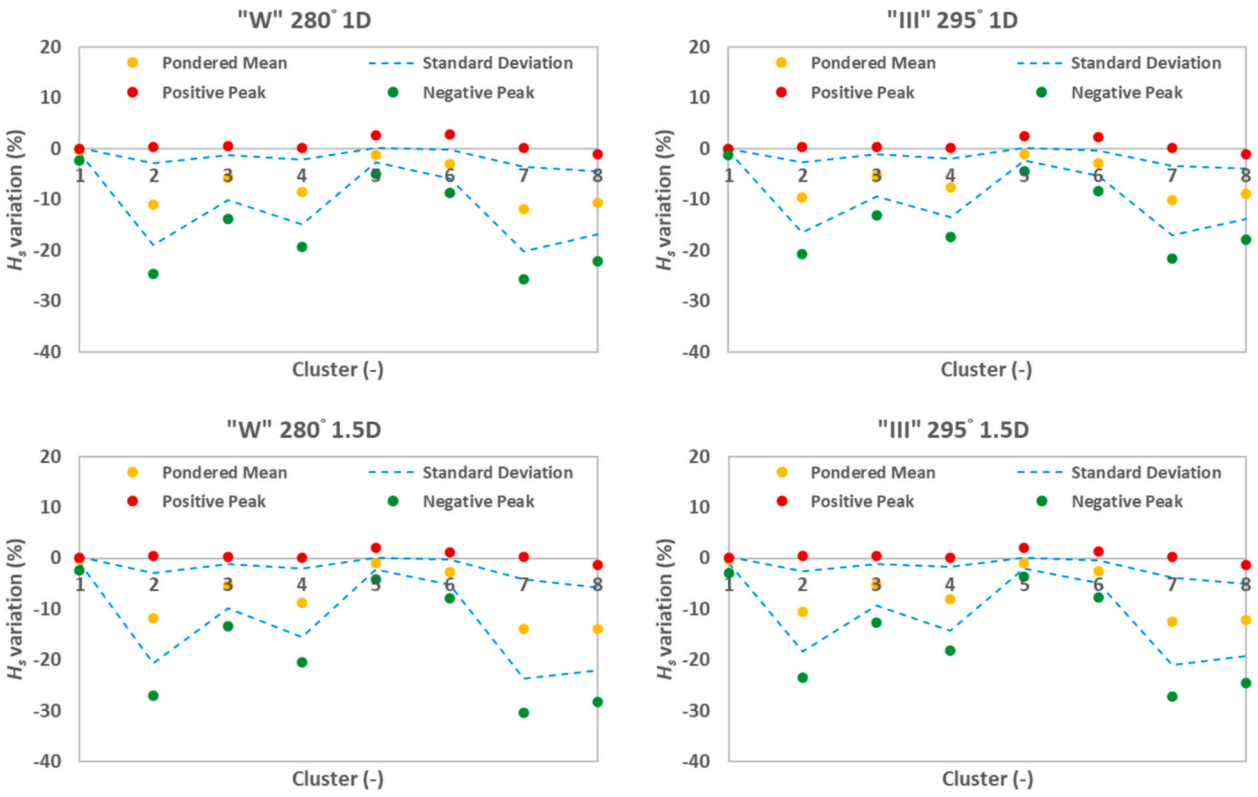

Fig. 12. – Statistical parameters of the *VI* metric for different clusters and park layouts, along the nearshore projection line.

clusters 3 and 5 exhibit a reduced variation at the 0.0 to 0.5 km range, while cluster 7, due to the larger *Dir*, demonstrated a greater wake effect even within this range. Secondly, there was a generally greater reduction of H_s with increasing tidal level, apart from cluster 1 (faster energy decrements with lower T_p). This seems to benefit the "intermediate" clusters (e.g., 3 and 7) – negative *VIs* close to −30 % –, but is not attributed to power absorption increase. The most suitable justification derives from shallow water-related phenomena like wave-breaking or bottom friction. This agrees with the computed H_s values, which increased with the tidal level (reduced energy losses), as addressed in [81]. Hence, the relative variations can be proportionally larger at higher tidal levels, as the influence of these phenomena is progressively less significant. Thirdly, there was a sharp shift towards a flat horizontal curve for the Zero level, mainly near the river mouth (after 2.5 km). Although this can be affected by model accuracy, the low tidal level may expose these areas, in agreement with fishermen remarks mentioned previously. Lastly, punctual positive *VIs* were again identified, mainly for cluster 5, at the 1.0 to 1.5 km range and at the river mouth area. The magnitudes remain virtually negligible for clusters other than 5, but the influence of the farm and the local water depth ought to be further conferred, in the future.

5. Discussion

In brief, the wave farm considered two parks – standalone Farm 1 and Farm 2, and the combined Farm 1,2 – of up to 150 B-OFs, which were placed at the case study's Northwest region, in accordance to the local bathymetry and marine restrictions. While most of the original model configurations were conserved, a mesh convergence was required to define the grid cell resolution, leading to a 3 × 3 m^2 setup. Eight representative sea-state clusters were selected, based on a K-Means analysis. Wave energy conversion and attenuation were evaluated through the CF, *AEP*, *q*-factor and *VI* metrics.

5.1. Complementary study remarks

It was observed that Farm 1 tends to contribute slightly more to the *AEP* than Farm 2 due to the distinct local wave conditions of the two sites. However, there is an equally pertinent and recurrent reduction upon comparing the standalone parks with their counterparts from Farm 1,2. This highlights the importance of park effects such as the "shadowing" effect by Farm 1 onto Farm 2. The total *AEP* reductions inherent to this effect, as seen in Fig. 8, range from 3.19 % to 8.92 %, in agreement with the local impact outcomes.

On farm orientation, unlike "W", the aligned B-OFs in "III" tend to directly "shadow" one another, going from the waveward rows to the leeward rows, Fig. 9 and Table 6, in agreement with other studies [39]. The farm configurations and complex near-field interference pattern play an important role, as perceivable from Fig. 9's analysis on the B-OF farm's local impact. One should consider that from "W" to "III" only the 2nd and 4th rows are shifted, which significantly affects the former row. Also, a greater perpendicular alignment of the parks with the incoming *Dir* favours a greater exposure of the B-OFs to incoming wave action, which is advantageous towards energy absorption. However, for the "III" configuration, the inter-row "shadowing" projection is exacerbated for the same reason, resulting in a delicate balance between wave and "shadowing" exposure that leads to "III" 295° surpassing "III" 280°. Due to the shoreline distance and the bathymetric profile, the wake effect becomes quite diminished away from the B-OF farm.

Concerning layout and spacing, the outcomes in Table 7 are attributed to the aforementioned inter-device and inter-park "shadowing", which explains the *q*-factor increase for the pondered sum of standalone parks. Such an occurrence is expected from the restricted spacing available for the B-OFs, as a result of the imposed marine space limitations. In literature, for instance, a separation of 2D or more is generally recommended to avoid destructive interference patterns, while, here, the maximum viable spacing was 1.5D [82]. This is further corroborated by the increasing *AEP* going from 1D to 1.5D. Even so, the effect exhibits

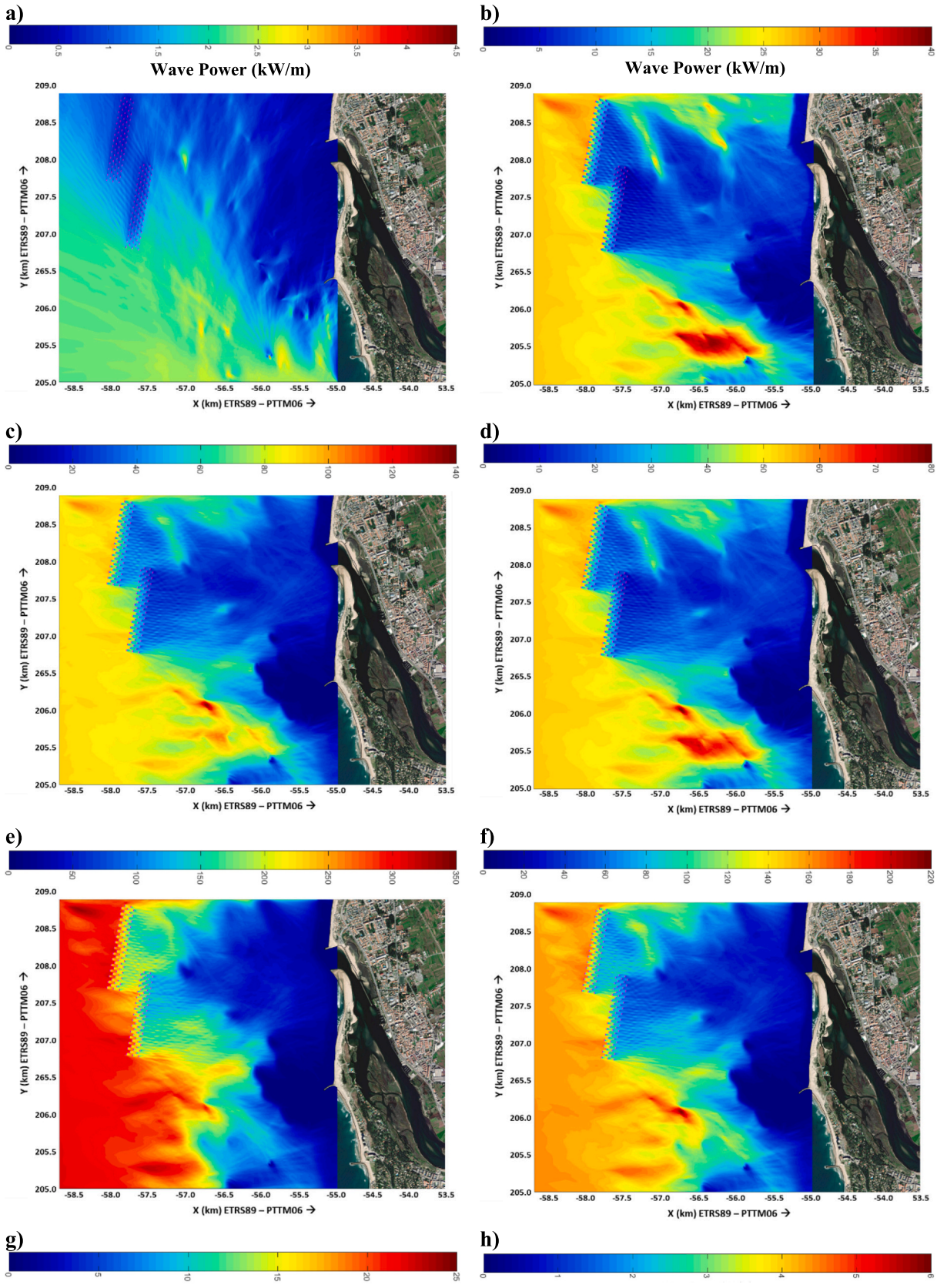

Fig. 13. – Wave power distribution across the case study region and with the selected B-OF farm, for clusters a) 1 through to h) 8, by that order.

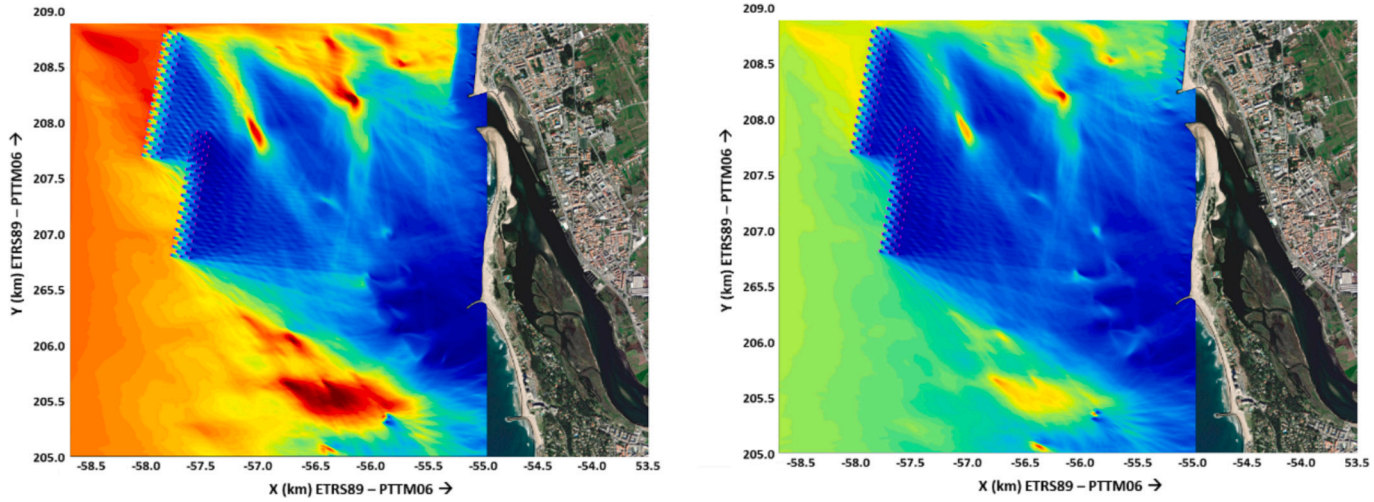

Fig. 13. (*continued*).

some changeability, as it negatively affects less the "W" configurations. The *q*-factor magnitudes appear to follow the variation of $H_s - T_p$ values. Moreover, punctual positive *VI* peaks of small magnitude (below 3 %) were identified from clusters 5 and 6, which exhibit the largest $H_s - T_p$ combinations. Even so, they should be interpreted with caution by considering: *i*) park-induced alignment of incoming waves overlapping with the original wave *Dir*, which re-direct the wake regions away from the river mouth (North) and 1.0 to 1.5 km range; *ii*) local depth, which is particularly shallow at these two locations and can affect the numerical model's accuracy, as well as exacerbate any local variations (shallow water conditions restrict the maximum non-breaking wave height).

On Fig. 15's *AEP* and CF values, three main factors contribute towards the observed outcomes. First, cluster 5 has a virtually null contribution for the 1 MW variant, Fig. 15a-ii, as the $H_s - T_p$ combination exceeds its power matrix range (survival mode). In SNL-SWAN, this yields a null power output. Punctual occurrences were also observed in the 2.5 MW version, as well as for cluster 6 in both variants, although several units absorbed energy. Secondly, the lower power matrix values associated with each $H_s - T_p$ values further reduced the *AEP*s for the 1 MW and 2.5 MW variants, except for clusters 1 and 8. Thirdly, there were distinct overlapping patterns between the $H_s - T_p$ from the power matrices and the clusters (power versus resource matrix), also evident from the CF values. While these remain somewhat modest under the reference range from the WaveRoller® – 0.25 to 0.50 [55] –, one should consider that *i*) this comparison is established between a standalone WaveRoller® (commercial) and a farm with 150 units (this study) under specific wave conditions, *ii*) public access to a complete WaveRoller® power matrix is difficult due to intellectual property restrictions, and *iii*) the inter-row "shadowing" significantly reduces the absorbed energy at the leeward rows, even if the waveward rows exhibit high *CF*s. Furthermore, the farm's role towards promoting coastal protection should also be considered alongside energy conversion.

Concerning the tidal levels, the standalone Farm 1 and Farm 2 again yielded slightly higher *CF*s and *q*-factors than their Farm 1,2 counterparts. Nevertheless, SNL-SWAN's limitations should, again, be accounted for. Since a B-OF or OWSC device is submerged, varying water levels affect its degree of submergence, which ought to influence the wave-structure interactions (e.g., incoming wave velocity profile along the WEC's flap) and, consequently, the absorbed energy. This is not replicated in SNL-SWAN and represents a key upgrade for future studies. Furthermore, it is worth highlighting some economic considerations. Cost inherent to the number of units (economies of scale versus installation expenditures), submerged cable extension (should increase with device spacing), accessibility (distance between WECs and to shore), generator rating (installed capacity investment) and operational efficiency (life-cycle) can influence the final decision-making process, and ought to be evaluated in future studies.

5.2. Study limitations and contributions

Looking at the final outcomes of this study, it becomes clear that there is a noteworthy potential in terms of implementing a wave energy farm for the Esposende nearshore region, so long as certain restrictions and premises are conserved. This follows on previous research from literature that has also focused on exploring the potential synergies of wave energy farms for coastal protection. For example, Carballo and Iglesias [67] investigated the impact of various layouts of WaveCat arrays (a lateral overtopping WEC) on the nearshore wave climate using the SWAN wave propagation model. Their study concluded that the presence of the farm led to reductions of up to 20 % in nearshore wave power. Abanades et al. [83,84] examined the effects of a wave farm on the profile of Perranporth Beach (UK) by integrating SWAN and XBeach morphodynamic model. They found that the presence of the wave farm contributed to reducing beach erosion by as much as 50 %. Bergillos et al. [85] evaluated the potential synergies of WaveCat arrays in mitigating coastal flooding. Their study determined that the presence of the wave farm mitigates flooding, particularly when the wedge angle of the WECs is 60°. These references provide a suitable range for the wave attenuation computed in this study, as H_s reductions of up to 30 %, in absolute values, were reported. However, despite the relevance of these findings, the preceding studies treated the WECs as obstacles with a constant transmission coefficient and examined a very limited number of sea-states, as outlined in other studies mentioned in the Introduction. Therefore, this research addresses these limitations by modelling WEC energy absorption using a frequency-based transmission coefficient – SNL-SWAN – dependent on the power matrix of the device and considering a broader range of sea-states representative of the annual wave conditions, in the region, based on a statistically robust and data-conservative methodology.

Furthermore, for the particular case of Esposende, no studies have thus far been conducted to incorporate a wave energy farm with the degree of detail and scope of this study. Also, the main source of coastal protection evaluation derives from the aforementioned rehabilitation study of the Ofir sandspit, which was based on experimental tests and numerical modelling with XBeach coupled with SWAN. This enabled a morphodynamic analyses adjacent to the shoreline, for which standalone SWAN exhibits poor accuracy. This greatly justified the nearshore projection line's distant position from the shoreline. Additionally, the sea-states considered in the rehabilitation study differ from the ones in this paper, and the former was mostly focused on estimating

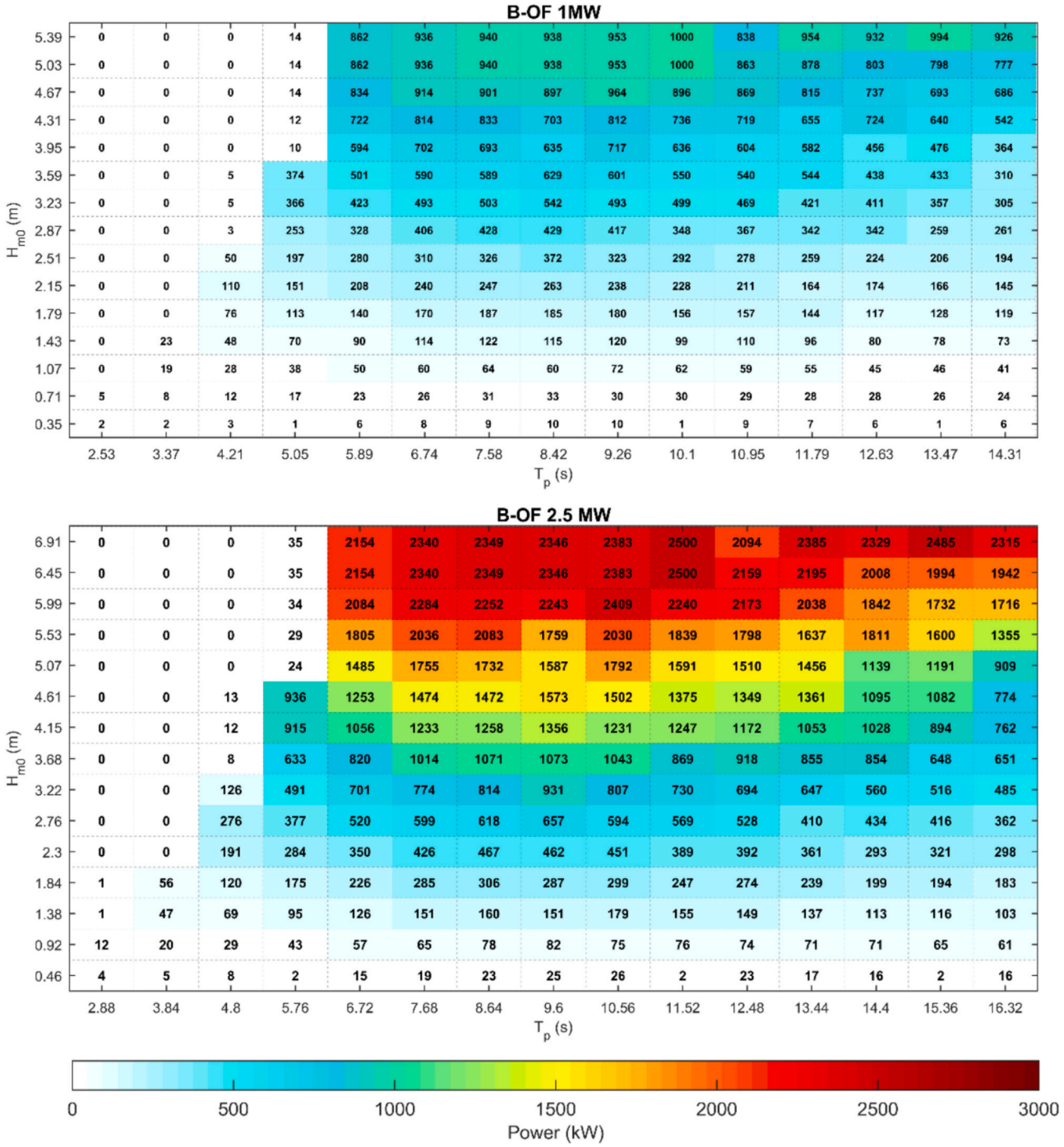

Fig. 14. – B-OF power matrices with ratings 1 MW and 2.5 MW.

overtopping, erosion/accretion and flow velocity change occurrences. Hence, a comparison in terms of wave attenuation outcomes between both studies should be interpreted with caution. With this in mind, it is worth noting that some estimates were made for wave attenuation. By resorting to the *VI* metric defined in this study and applying it to the tests from the rehabilitation study (cases without the breakwater structure versus those with the implanted breakwaters, see Sections 6 and 7 of the report [46]), it was possible to compute *VI* mean values for H_s of −1.07 % ±11.73 % to 3.68 % ±13.77 % and peak *VIs* of nearly −25 % (excluding outliers). Note that these values are, overall, of similar to lower magnitude than those obtained from the wave farm proposal, but exhibit significant variability, as they consider measurements from distinct nearshore locations and wave conditions.

As done with the rehabilitation study, there is also the prospect of a follow-up study in which the outputs of the SNL-SWAN simulations can be used as input for a XBeach model. This will enable an enhanced evaluation of the wave farm's nearshore impact in terms of coastal protection, morphodynamics, water flows and sediment transport.

6. Conclusions

This paper addressed a dual wave farm proposal, based on generic OWSC-type WECs, for the nearshore Esposende. Whilst accounting for local marine space limitations and technological characteristics, it was feasible to explore distinct farm configurations, park layouts and device ratings under a statistically representative set of wave conditions for

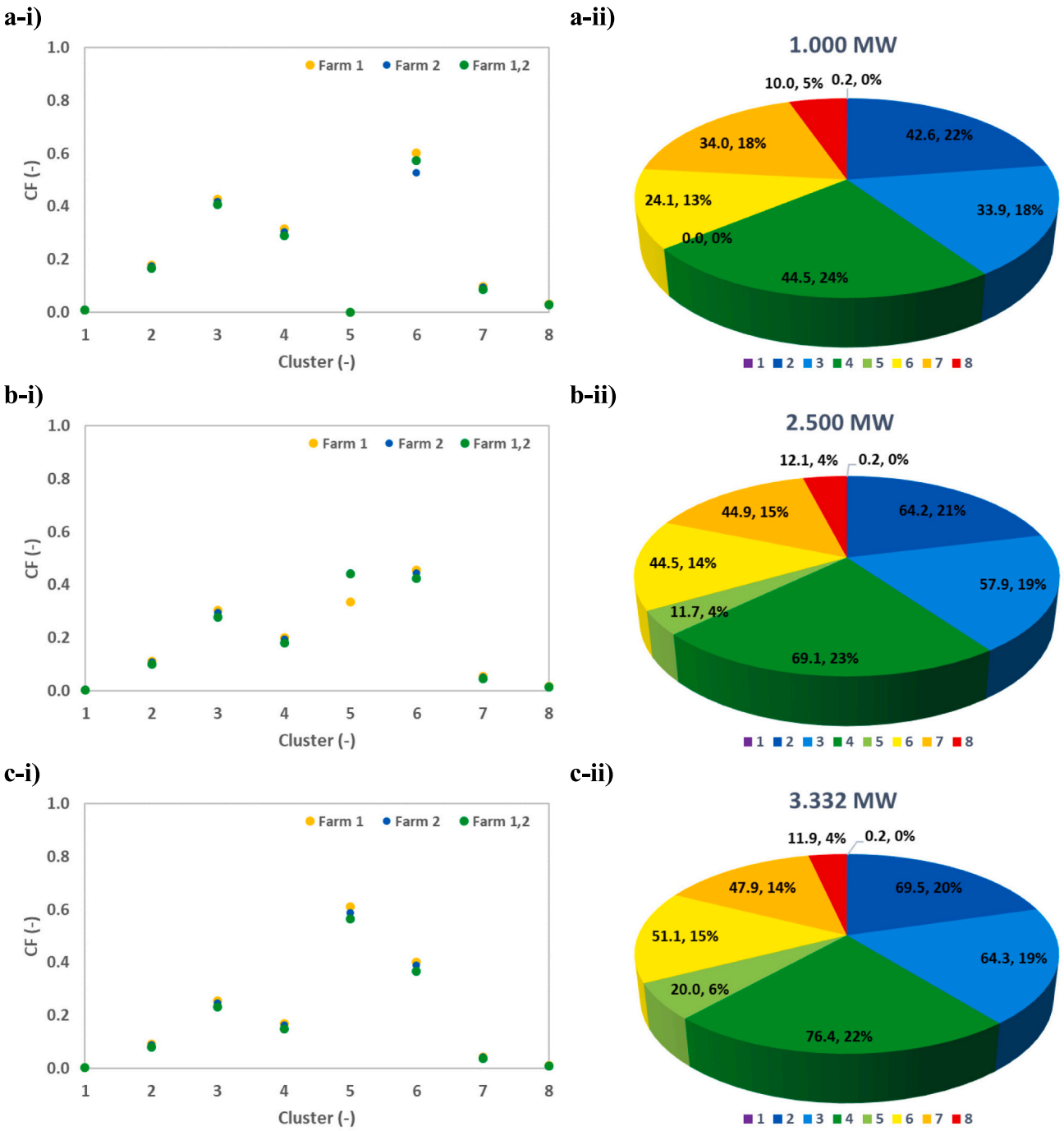

Fig. 15. – Capacity factors (i) and *AEP* distribution (ii) per cluster for the "W" 280° 1.5D layout, considering the power matrices with rating a) 1 MW, b) 2.5 MW and c) 3.332 MW.

varying tidal levels. While robust state-of-the-art approaches were applied, from the SNL-SWAN numerical model to K-Means clustering, the encompassing number of variable combinations and practical considerations showcase the novelty and reliability of this work.

Results point towards:

- Improved performance for the "W" 280° and "III" 295 °configurations, with *AEP*s of up to 341.353 GWh/yr and 316.351 GWh/yr, respectively. If one considers the average electricity consumption per capita in Esposende – about 3215 kWh in 2022, according to the national Pordata database –, the best configuration could meet the annual needs of over 100,000 habitants;
- Clusters 2 to 4 as the main energy absorption contributors, due to a large number of data points with beneficial overlap between the inherent wave conditions and the original B-OF power matrix. These values assume the largest inter-device spacing – 1.5D –, as the energy/power metrics systematically improved alongside increased spacing;
- Near-field interactions were always destructive (q-factors below 1) but varied in magnitude depending upon farm orientation towards the waves, inter-device spacing and alignment between rows. q-factors tended to increase with $H_s - T_p$, as well;

Metrics	Clusters	1	2	3	4	5	6	7	8	Pondered Mean Farm 1,2
q-factor (-)	ZH level	0.30	0.69	0.78	0.75	0.81	0.80	0.65	0.53	0.64
	LTWS level	0.31	0.69	0.78	0.75	0.82	0.79	0.65	0.52	0.64
	MSL level	0.35	0.68	0.77	0.74	0.83	0.79	0.64	0.52	0.64
	HTWS level	0.38	0.68	0.77	0.74	0.83	0.79	0.63	0.51	0.63
	HT level	0.39	0.67	0.76	0.74	0.83	0.78	0.63	0.51	0.63
CF (-)	ZH level	0.00	0.08	0.23	0.15	0.55	0.37	0.04	0.01	0.08
	LTWS level	0.00	0.08	0.23	0.15	0.56	0.37	0.04	0.01	0.08
	MSL level	0.00	0.08	0.23	0.15	0.57	0.37	0.04	0.01	0.08
	HTWS level	0.00	0.08	0.23	0.15	0.57	0.36	0.04	0.01	0.08
	HT level	0.00	0.08	0.23	0.15	0.56	0.36	0.04	0.01	0.08

Fig. 16. – *q*-factor and CF maps under varying tidal levels for farm 1,2 ("W" 280°, with 1.5 D spacing and 3.332 MW rating).

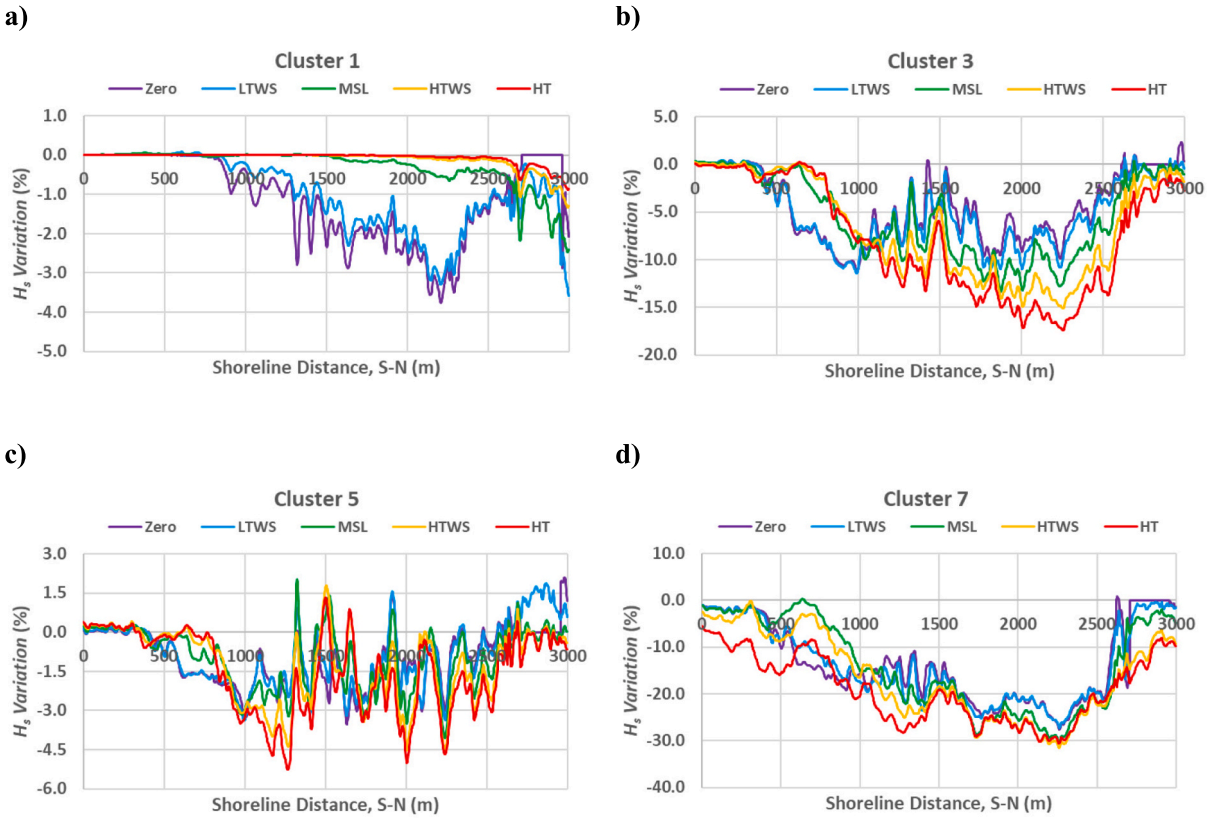

Fig. 17. – *VI* values along the nearshore projection line, under varying tidal levels, for clusters a) 1, b) 3, c) 5, d) and 7.

- While pondered mean *CF*s increased slightly for lower power ratings, from 0.078 to 0.144, they remain modest by comparison with the WaveRoller's® range. Also, standalone parks exhibited a slightly greater absorption capability, justified by inter-park "shadowing" of the combined farm;
- The farm's local impact was perceivable, especially with the increased area of influence from larger inter-device spacing. However, it mainly impacted H_s and *J*, and the farm's wake significantly diminished upon approaching the shoreline;
- While important wave height reductions were obtained – peak *VI*s beyond −25 % for H_s –, punctual increments were identified. The latter are associated with very shallow water zones along the nearshore projection – river mouth and 1.0 to 1.5 km range –, and should be interpreted with caution, given SNL-SWAN's limitations;
- The varying tidal level did not significantly alter the CF and *q*-factor values, ranging from just over 0.00 to 0.57 and 0.30 to 0.83, respectively and depending on the cluster. However, they affected the H_s *VI*s considerably, with an overall improvement being observed for higher tidal levels. Maximum absolute reductions of about 30 % were reported, influenced by the farm's wake effect and shallow water-related phenomena.

This paper forms the basis of a plausible proposal for a nearshore dual wave farm for Esposende, aimed at providing renewable energy to local communities whilst protecting the sensitive shoreline. While the comparison with the rehabilitation study has several limitations, the B-OF's wave attenuation was found to be of similar or even greater magnitude than that obtained from the breakwater-based solution. Nevertheless, future studies are required, namely to improve on the limitations of SNL-SWAN (e.g., modelling shoreline interactions, incorporating the river component, assessing the influence of currents and reproducing OWSC submergence with greater accuracy). Contact with

local communities and stakeholders will be pivotal towards a viable, endorsed, and enhanced proposal, in order to ensure a sound solution that benefits all interested parties whilst meeting energy demands and preserving the environment and meeting.

Funding

The authors acknowledge funding through the project Ocean3R – Reduce pressures, restore and regenerate the NW-Portuguese ocean and waters, with reference NORTE-01-0145-FEDER-000064. The authors further acknowledge financial support from the project ATLANTIDA – Platform for the monitoring of the North Atlantic Ocean and tools for the sustainable exploitation of the marine resources, with reference NORTE-01-0145-FEDER-000040, which is co-financed by the European Regional Development Fund (ERDF) through NORTE2020. F. Teixeira-Duarte also acknowledges the funding in the form of a Ph.D. scholarship grant by the Portuguese Foundation of Science and Technology (FCT), co-financed by the EU's ESF through the NORTE 2020 program, with reference 2020.09157.BD. V. Ramos was supported by the program of Stimulus of Scientific Employment Individual Support (CEECIND/03665/2018) from the FCT. F. V. C. Taveira-Pinto received funding in the form of a Ph.D. scholarship grand by the FCT with reference 2021.06629.BD.

CRediT authorship contribution statement

D. Clemente: Writing – original draft, Visualization, Validation, Software, Methodology, Investigation, Formal analysis, Data curation, Conceptualization. **V. Ramos:** Writing – review & editing, Visualization, Validation, Software, Resources, Methodology, Investigation, Formal analysis, Data curation, Conceptualization. **F. Teixeira-Duarte:** Writing – review & editing, Software, Methodology, Investigation, Formal analysis. **F.V.C. Taveira-Pinto:** Writing – review & editing, Visualization, Software, Methodology, Investigation, Formal analysis, Data curation. **P. Rosa-Santos:** Writing – review & editing, Validation, Supervision, Resources, Project administration, Investigation, Funding acquisition, Formal analysis, Data curation, Conceptualization. **F. Taveira-Pinto:** Writing – review & editing, Validation, Supervision, Resources, Project administration, Investigation, Funding acquisition, Formal analysis, Data curation, Conceptualization.

Declaration of competing interest

The authors declare the following financial interests/personal relationships which may be considered as potential competing interests: The authors report financial support was provided by the Foundation for Science and Technology (FCT) and by the European Regional Development Fund (ERDF).

Data availability

Data will be made available on request.

Acknowledgments

The authors would like to thank Prof. Fernanda Campos de Sousa from the Department of Civil Engineering – Mathematics division –, at the Faculty of Engineering of the University of Porto, for her support and expertise in the statistical analysis with the K-Means clustering technique. The authors would equally like to extend their gratitude to the Esposende City Hall for providing auxiliary information regarding the local marine space restrictions and current legislation.

Appendix A. Grid convergence summary

Table A1
– Grid convergence evaluation for absorbed power variations, under average wave conditions.

Grid cells	$7 \times 7\ m^2$	$6 \times 6\ m^2$	$5 \times 5\ m^2$	$4 \times 4\ m^2$	$3 \times 3\ m^2$
B-OF unit	(kW)	(%)	(%)	(%)	(%)
Row 1, Unit 1	368	−14.5	7.7	6.0	−5.7
Row 1, Unit 2	377	−14.6	8.7	−9.4	1.1
Row 1, Unit 3	387	−13.6	9.2	−11.2	1.0
Row 1, Unit 4	430	−21.6	8.7	−11.1	9.6
Row 1, Unit 5	307	12.2	−20.1	16.1	1.3
Row 1, Unit 6	346	−0.1	8.8	−3.1	−5.5
Row 1, Unit 7	305	10.7	2.4	−1.3	0.3
Row 1, Unit 8	347	−1.4	8.9	−2.1	−7.1
Row 1, Unit 9	306	10.9	9.0	−9.2	0.4
Row 1, Unit 10	319	8.2	9.1	6.6	−9.4
Row 2, Unit 1	265	−6.0	9.6	−11.0	9.1
Row 2, Unit 2	283	10.9	−15.9	4.8	−9.9
Row 2, Unit 3	276	0.7	7.3	−8.8	−1.9
Row 2, Unit 4	307	−9.9	7.9	−4.0	−9.6
Row 2, Unit 5	309	−6.2	−24.6	15.6	−1.4
Row 2, Unit 6	351	−31.6	10.6	−7.0	−2.7
Row 2, Unit 7	307	−16.0	3.4	−4.8	5.4
Row 2, Unit 8	348	−32.1	10.3	−9.3	6.9
Row 2, Unit 9	336	−2.9	−21.8	0.2	1.9
Row 2, Unit 10	365	−17.1	5.1	−9.6	4.8
Row 3, Unit 1	254	−16.1	−4.0	1.6	−0.9
Row 3, Unit 2	166	5.4	1.1	−6.2	4.4
Row 3, Unit 3	185	−8.4	1.5	−2.3	−1.5
Row 3, Unit 4	162	8.9	−2.0	−8.5	3.6
Row 3, Unit 5	202	−14.1	15.9	−19.6	2.6
Row 3, Unit 6	174	3.2	−24.0	12.6	2.0
Row 3, Unit 7	205	−14.3	7.3	−6.4	−7.3
Row 3, Unit 8	173	3.3	0.5	−11.8	4.8

(*continued on next page*)

Table A1 (*continued*)

Grid cells	$7 \times 7\ m^2$	$6 \times 6\ m^2$	$5 \times 5\ m^2$	$4 \times 4\ m^2$	$3 \times 3\ m^2$
Row 3, Unit 9	213	−5.6	−8.3	4.2	−2.9
Row 3, Unit 10	213	−6.1	−17.1	7.6	−1.9

References

[1] IEA-OES. Annual Report: an Overview of ocean energy activities in 2022. Lisboa, Portugal: ocean energy systems. 2023.
[2] Ocean Energy Europe. Ocean Energy: Key trends and statistics 2022. Brussels, Belgium: Ocean Energy Europe; 2023.
[3] Majidi AG, Ramos V, Giannini G, Rosa Santos P, das Neves L, Taveira-Pinto F.. The impact of climate change on the wave energy resource potential of the Atlantic coast of Iberian Peninsula. Ocean Eng 2023:115451. https://doi.org/10.1016/j.oceaneng.2023.115451.
[4] Ramos V, López M, Taveira-Pinto F, Rosa-Santos P. Influence of the wave climate seasonality on the performance of a wave energy converter: a case study. Energy 2017;135:303–16. https://doi.org/10.1016/j.energy.2017.06.080.
[5] APREN. Electricity generation by energy sources in Mainland Portugal in 2023. APREN - Prod 2023. https://www.apren.pt/en/renewable-energies/production/ (accessed July 26, 2023).
[6] European Comission. REPowerEU: Affordable, secure and sustainable energy for Europe. 2022. https://commission.europa.eu/strategy-and-policy/priorities-2019-2024/european-green-deal/repowereu-affordable-secure-and-sustainable-energy-europe_en (accessed July 26, 2023).
[7] Clemente D, Rosa-Santos P, Taveira-Pinto F. On the potential synergies and applications of wave energy converters: a review. Renew Sust Energ Rev 2021;135:17. https://doi.org/10.1016/j.rser.2020.110162.
[8] Clemente D, Rosa-Santos P, Ferradosa T, Taveira-Pinto F. Wave energy conversion energizing offshore aquaculture: prospects along the Portuguese coastline. Renew Energy 2023;204:347–58. https://doi.org/10.1016/j.renene.2023.01.009.
[9] Azinheira G, Segurado R, Costa M. Is renewable energy-powered desalination a viable solution for water stressed regions? A case study in Algarve. Portugal Energies 2019;12:18. https://doi.org/10.3390/en12244651.
[10] Iglesias G, López M, Carballo R, Castro A, Fraguela JA, Frigaard P. Wave energy potential in Galicia (NW Spain). Renew Energy 2009;34:2323–33. https://doi.org/10.1016/j.renene.2009.03.030.
[11] Pontes MT, Aguiar R, Oliveira Pires H. A nearshore wave energy atlas for Portugal. J Offshore Mech Arct Eng 2003;127:249–55. https://doi.org/10.1115/1.1951779.
[12] Rusu E, Guedes Soares C. Numerical modelling to estimate the spatial distribution of the wave energy in the Portuguese nearshore. Renew Energy 2009;34:1501–16. https://doi.org/10.1016/j.renene.2008.10.027.
[13] Mota P, Pinto JP. Wave energy potential along the western Portuguese coast. Renew Energy 2014;71:8–17. https://doi.org/10.1016/j.renene.2014.02.039.
[14] Rusu L. The near future expected wave power in the coastal environment of the Iberian Peninsula. Renew Energy 2022;195:657–69. https://doi.org/10.1016/J.RENENE.2022.06.047.
[15] Arguilé-Pérez B, Ribeiro AS, Costoya X, deCastro M, Gómez-Gesteira M. Suitability of wave energy converters in northwestern Spain under the near future winter wave climate. Energy 2023:29. https://doi.org/10.1016/j.energy.2023.127957.
[16] Offshore Energy. WaveRoller emerges from the depths of Atlantic. 2021. https://www.offshore-energy.biz/waveroller-emerges-from-the-depths-of-atlantic/?utm_source=marineenergy&utm_medium=email&utm_campaign=newsletter_2021-08-03 (accessed August 3, 2021).
[17] Garanovic A. CorPower wraps up preparatory trials ahead of C4 wave energy device deployment. Offshore. Energy 2023. https://www.offshore-energy.biz/corpower-wraps-up-preparatory-trials-ahead-of-c4-wave-energy-device-deployment/ [accessed March 3, 2023].
[18] Eco Wave Power. Eco wave power announces strategic collaboration with Painhas engineering and construction company for its 20MW Portugal project. Eco Wave Power 2020. https://www.ecowavepower.com/eco-wave-power-announces-strategic-collaboration-with-painhas-engineering-and-construction-company-for-its-portugal-project/ [accessed February 6, 2021].
[19] XXIII Portuguese Government. Preliminary proposal of specialized areas and seaports connected to the Nacional electricity grid and transport. Portugal: grupo de Trabalho para o planeamento e operacionalização de centros electroprodutores baseados em fontes renováveis de origem ou localização oceânica. 2022.
[20] Clark CE, Miller A, DuPont B. An analytical cost model for co-located floating wind-wave energy arrays. Renew Energy 2019;132:885–97. https://doi.org/10.1016/j.renene.2018.08.043.
[21] Astariz S, Perez-Collazo C, Abanades J, Iglesias G. Hybrid wave and offshore wind farms: a comparative case study of co-located layouts. Int J Mar Energy 2016;15:2–16. https://doi.org/10.1016/j.ijome.2016.04.016.
[22] Astariz S, Iglesias G. Enhancing wave energy competitiveness through co-located wind and wave energy farms. RevShadow Effect Energies 2015;8:7344–66. https://doi.org/10.3390/en8077344.
[23] Teixeira-Duarte F, Ramos V, Rosa-Santos P, Taveira-Pinto F. Multi-objective decision tool for the assessment of co-located wave-wind offshore floating energy parks. Ocean Eng 2024;292:116449. https://doi.org/10.1016/j.oceaneng.2023.116449.
[24] Liu L, Yang X, Zhao L, Hong H, Cui H, Duan J, et al. Nodding duck structure multi-track directional freestanding triboelectric nanogenerator toward low-frequency ocean wave energy harvesting. ACS Nano 2021:16. https://doi.org/10.1021/acsnano.1c00345.
[25] Clemente D, Rodrigues C, Esteves R, Correia J, Pereira AM, Ventura JO, et al. Experimental performance analysis of a hybrid wave energy harvesting system combining E-motions with triboelectric nanogenerators. J Mar Sci Eng 2022;10:26. https://doi.org/10.3390/jmse10121924.
[26] Carapellese F, Pasta E, Sirigu SA, Faedo N. SWINGO: conceptualisation, modelling, and control of a swinging omnidirectional wave energy converter. Mech Syst Signal Process 2023;197:27. https://doi.org/10.1016/j.ymssp.2023.110356.
[27] Clemente D, Calheiros-Cabral T, Rosa-Santos P, Taveira-Pinto F. Hydraulic and structural assessment of a rubble-mound breakwater with a hybrid wave energy converter. J Mar Sci Eng 2021;9:17. https://doi.org/10.3390/jmse9090922.
[28] Zheng S, Zhang Y. Analytical study on wave power extraction from a hybrid wave energy converter. Ocean Eng 2018;165:252–63. https://doi.org/10.1016/j.oceaneng.2018.07.021.
[29] Ghafari HR, Ghassemi H, Neisi A. Power matrix and dynamic response of the hybrid wavestar-deepcwind platform under different diameters and regular wave conditions. Ocean Eng 2022;247:17. https://doi.org/10.1016/j.oceaneng.2022.110734.
[30] Abanades J, Flor-Blanco G, Flor G, Iglesias G. Dual wave farms for energy production and coastal protection. Ocean Coast Manag 2018;160:18–29. https://doi.org/10.1016/j.ocecoaman.2018.03.038.
[31] Abanades J, Greaves D, Iglesias G. Coastal defence using wave farms: the role of farm-to-coast distance. Renew Energy 2015;75:572–82. https://doi.org/10.1016/j.renene.2014.10.048.
[32] Balitsky P, Quartier N, Stratigaki V, Verao Fernandez G, Vasarmidis P, Troch P. Analysing the near-field effects and the power production of near-shore WEC array using a new wave-to-wire model. Water 2019;11:30. https://doi.org/10.3390/w11061137.
[33] Bergillos RJ, López-Ruiz A, Medina-López E, Moñino A, Ortega-Sánchez M. The role of wave energy converter farms on coastal protection in eroding deltas, Guadalfeo, southern Spain. J Clean Prod 2018;171:356–67. https://doi.org/10.1016/j.jclepro.2017.10.018.
[34] Teixeira-Duarte F, Clemente D, Giannini G, Rosa-Santos P, Taveira-Pinto F. Review on layout optimization strategies of offshore parks for wave energy converters. Renew Sust Energ Rev 2022;163:19. https://doi.org/10.1016/j.rser.2022.112513.
[35] Clemente D, Teixeira-Duarte F, Rosa-Santos P, Taveira-Pinto F. Advancements on optimization algorithms applied to wave energy assessment: an overview on wave climate and energy resource. Energies 2023;16:28. https://doi.org/10.3390/en16124660.
[36] Deltares. SWAN - users manual, swan cycle III version41; 2017. p. 20.
[37] Deltares. Delft3D-WAVE simulation of short-crested waves with SWAN: User manual, hydro-morphodynamics. 2014.
[38] SNL. Project overview — SNL-SWAN. 2020.
[39] Onea F, Rusu L, Carp GB, Rusu E. Wave farms impact on the coastal processes—a case study area in the Portuguese nearshore. J Mar Sci Eng 2021;9:262. https://doi.org/10.3390/jmse9030262.
[40] Fanti V. Application of snl-swan model on the effect of wave farms in the wave propagation. Master's Thesis. Faculty of Science and Technology, University of Algarve; 2019.
[41] Fanti V, Jacob J, Pacheco A, Fortes CJEM, Didier E. Effects of varying the transmission coefficient in SNL-SWAN for a wave farm in Peniche. Dev Renew Energ Offshore 2020:8. CRC Press.
[42] Ruehl K, Porter A, Posner A, Roberts J. Development of SNL-SWAN, a validated wave energy converter Array modeling tool. In: Proc 10th Eur. Wave tidal Energy Conf. EWTEC 2013, Aalborg, Denmark: Tethys; 2013. p. 7.
[43] Ruehl K, Porter A, Chartrand C, Smith H, Chang G, Roberts J. Development, verification and application of the SNL-SWAN open source wave farm code. In: Proc 11th Eur. Wave tidal energy conf. EWTEC 2015. vol. 11; 2015. Nantes, France.
[44] Lo Re C, Manno G, Basile M, Ciraolo G. The opportunity of using wave energy converters in a Mediterranean hot spot. Renew Energy 2022;196:1095–114. https://doi.org/10.1016/j.renene.2022.07.010.
[45] Chang G, Ruehl K, Jones CA, Roberts J, Chartrand C. Numerical modeling of the effects of wave energy converter characteristics on nearshore wave conditions. Renew Energy 2016;89:636–48. https://doi.org/10.1016/j.renene.2015.12.048.
[46] IHRH, Minho University, Esposende City Hall. Risk characterization study and intervention plan for protecting the Ofir sandbank and Cávado mouth. Esposende, Portugal: Faculty of Engineering of the University of Porto; 2021.
[47] Surf-Forecast. Esposende surf forecast and surf reports (Douro & Minho, Portugal). Surf-forecast. 2023. https://www.surf-forecast.com/breaks/Esposende/surf-stats (accessed March 30, 2023).
[48] ABPmer. Explore data - seastates. 2021. https://www.seastates.net/explore-data/ (accessed March 30, 2023).

[49] Tides4Fishing. Tides4fishing 2023 for Esposende, Braga. 2023. https://tabuademares.com/pt/braga/esposende [accessed August 15, 2023].
[50] DGRM. Geoportal do Mar Português. 2023. https://webgis.dgrm.mm.gov.pt/portal/apps/webappviewer/index.html?id=df8accb510bc4f33963d9b03bf3674b8 (accessed February 28, 2023).
[51] ICNF. Littoral North Natural Park. Esposende. Portugal: Instituto da Conservação da Natureza e das Florestas; 2007.
[52] Geoportal HI. Hydrographic institute. Hidrogr Mais. 2023. https://geomar.hidrografico.pt/ (accessed August 15, 2023).
[53] de Falcão AFO. Wave energy utilization: a review of the technologies. Renew Sust Energ Rev 2010;14:899–918. https://doi.org/10.1016/j.rser.2009.11.003.
[54] Babarit A, Hals J, Muliawan MJ, Kurniawan A, Moan T, Krokstad J. Numerical benchmarking study of a selection of wave energy converters. Renew Energy 2012;41:44–63. https://doi.org/10.1016/j.renene.2011.10.002.
[55] AW-Energy Oy. WaveRoller – AW-energy Oy. 2022. https://aw-energy.com/waveroller/ (accessed August 10, 2022).
[56] EEA. Natura 2000 - litoral norte. biodiversityEuropa. 2021. https://biodiversity.europa.eu/natura2000/sites/site (accessed August 15, 2023).
[57] Rodrigues J, Guimarães M, Villasante S, Sousa Pinto I. Workshop report "Parque Natural do Litoral Norte: que futuros?" Esposende. Portugal: CIIMAR; 2019.
[58] AW-Energy. Pilot waveroller power plant operational by mid-2012. AW-Energy 2010. https://aw-energy.com/pilot-waveroller-power-plant-operational-by-mid-2012/ [accessed August 15, 2023].
[59] Liljelund J. WaveRoller - plug into wave energy. 2016.
[60] Ocean Energy Systems. Offshore aquaculture: A market for ocean renewable Energy. Europe: OES; 2022.
[61] LNEG. OffShorePlan – Planeamento do aproveitamento das energias Renováveis offshore em Portugal. 2020. https://offshoreplan.lneg.pt/ (accessed August 23, 2023).
[62] Iglesias G, Carballo R. Wave farm impact: the role of farm-to-coast distance. Renew Energy 2014;69:375–85. https://doi.org/10.1016/j.renene.2014.03.059.
[63] David DR, Rijnsdorp DP, Hansen JE, Lowe RJ, Buckley ML. Predicting coastal impacts by wave farms: a comparison of wave-averaged and wave-resolving models. Renew Energy 2021:33. https://doi.org/10.1016/j.renene.2021.11.048.
[64] Ramos V, Ringwood JV. Exploring the utility and effectiveness of the IEC (international electrotechnical commission) wave energy resource assessment and characterisation standard: a case study. Energy 2016;107:15. https://doi.org/10.1016/j.energy.2016.04.053.
[65] Majidi AG, Ramos V, Santos P, Neves L, Taveira-Pinto F. The impact of the SWAN model calibration on the energy production of wave energy converter systems. In: BoA 7th Eur. Congr. Int. Assoc. hydro-environ. Eng. Res. Athens, Greece: IAHR; 2022. p. 2.
[66] Akpınar A, Bingölbali B, Van Vledder Gph. Long-term analysis of wave power potential in the Black sea, based on 31-year SWAN simulations. Ocean Eng 2017;130:482–97. https://doi.org/10.1016/j.oceaneng.2016.12.023.
[67] Carballo R, Iglesias G. Wave farm impact based on realistic wave-WEC interaction. Energy 2013;51:216–29. https://doi.org/10.1016/j.energy.2012.12.040.
[68] Bergillos RJ, Rodriguez-Delgado C, Iglesias G. Wave farm impacts on coastal flooding under sea-level rise: a case study in southern Spain. Sci Total Environ 2019;653:1522–31. https://doi.org/10.1016/j.scitotenv.2018.10.422.
[69] Astariz S, Abanades J, Perez-Collazo C, Iglesias G. Improving wind farm accessibility for operation & maintenance through a co-located wave farm: influence of layout and wave climate. Energy Convers Manag 2015;95:229–41. https://doi.org/10.1016/j.enconman.2015.02.040.
[70] Luczko E, Robertson B, Bailey H, Hiles C, Buckham B. Representing non-linear wave energy converters in coastal wave models. Renew Energy 2018;118:376–85. https://doi.org/10.1016/j.renene.2017.11.040.
[71] Porter A, Ruehl K, Chartrand C. Further development of SNL-SWAN, a validated wave energy converter array modelling tool. In: Proc. 2nd mar. Energy technol; 2014. p. 9. Symp., Seattle, USA.
[72] Porter A, Ruehl K, Chartrand C, Smith H. Development and release of the open-source wave climate environment assessment tool SNL-SWAN. In: Proc. 3rd mar. Energy technol; 2015. p. 5. Symp., Washington DC, USA.
[73] Ramos V, López M, Taveira-Pinto F, Rosa-Santos P. Performance assessment of the CECO wave energy converter: water depth influence. Renew Energy 2018;117:341–56. https://doi.org/10.1016/j.renene.2017.10.064.
[74] Deltares. QUICKIN - Generation and manipulation of grid-related parame- ters such as bathymetry, initial conditions and rough- ness: User manual, hydro-morphodynamics & water quality. 2018.
[75] Pecher A, Kofoed JP, editors. Handbook of ocean wave energy. vol. 7. Cham: Springer International Publishing; 2017. https://doi.org/10.1007/978-3-319-39889-1.
[76] Wang D, Jin S, Hann M, Conley D, Collins K, Greaves D. Power output estimation of a two-body hinged raft wave energy converter using HF radar measured representative sea states at wave hub in the UK. Renew Energy 2023;202:103–15. https://doi.org/10.1016/j.renene.2022.11.048.
[77] Wang D, Greaves D, Conley D, Hann M, Collins K, Jin S. Power output estimation of WECs by using K-means clustered HF radar representative sea states. In: Proc 14th Eur. Wave tidal energy Conf; 2021. p. 9. Plymouth, UK.
[78] IBM. IBM SPSS Software. 2022.
[79] Ramos V, Giannini G, Calheiros-Cabral T, Rosa-Santos P, Taveira-Pinto F. An integrated approach to assessing the wave potential for the energy supply of ports: a case study. J Mar Sci Eng 2022;10:24. https://doi.org/10.3390/jmse10121989.
[80] Oliveira-Pinto S, Rosa-Santos P, Taveira-Pinto F. Electricity supply to offshore oil and gas platforms from renewable ocean wave energy: overview and case study analysis. Energy Convers Manag 2019;186:556–69. https://doi.org/10.1016/j.enconman.2019.02.050.
[81] Rodriguez-Delgado C, Bergillos RJ, Iglesias G. Dual wave farms for energy production and coastal protection under sea level rise. J Clean Prod 2019. https://doi.org/10.1016/j.jclepro.2019.03.058.
[82] Benites-Munoz D, Huang L, Thomas G. Optimal array arrangement of oscillating wave surge converters: an analysis based on three devices. Renew Energy 2024;222:119825. https://doi.org/10.1016/j.renene.2023.119825.
[83] Abanades J, Greaves D, Iglesias G. Coastal defence through wave farms. Coast Eng 2014;91:299–307. https://doi.org/10.1016/j.coastaleng.2014.06.009.
[84] Abanades J, Greaves D, Iglesias G. Wave farm impact on the beach profile: a case study. Coast Eng 2014;86:36–44. https://doi.org/10.1016/j.coastaleng.2014.01.008.
[85] Bergillos RJ, Rodriguez-Delgado C, Allen J, Iglesias G. Wave energy converter geometry for coastal flooding mitigation. Sci Total Environ 2019. https://doi.org/10.1016/j.scitotenv.2019.03.022.